

Key Points:

- Descriptive oceanography of the Levantine Intermediate Water formation zone using an *in-situ* multiplatform approach
- Competition between two source regions to supply the Mediterranean overturning circulation in Levantine Intermediate Water
- The Cretan Sea is the most abundant source, supported by increasingly saltier waters coming from the Levantine Sea

Correspondence to:

V. Taillandier,
taillandier@obs-vlfr.fr

Citation:

Taillandier, V., D'Ortenzio, F., Prieur, L., Conan, P., Coppola, L., Cornec, M., et al. (2022). Sources of the Levantine intermediate water in winter 2019. *Journal of Geophysical Research: Oceans*, 127, e2021JC017506. <https://doi.org/10.1029/2021JC017506>

Received 23 APR 2021

Accepted 4 JUN 2022









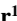






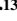

Author Contributions:

Conceptualization: V. Taillandier, F. D'Ortenzio, L. Prieur
Data curation: V. Taillandier
Formal analysis: V. Taillandier, L. Prieur
Funding acquisition: F. D'Ortenzio
Investigation: V. Taillandier, F. D'Ortenzio
Methodology: V. Taillandier, F. D'Ortenzio, L. Prieur
Validation: L. Prieur
Visualization: V. Taillandier
Writing – original draft: V. Taillandier, F. D'Ortenzio

© 2022 The Authors.

This is an open access article under the terms of the [Creative Commons Attribution-NonCommercial License](#), which permits use, distribution and reproduction in any medium, provided the original work is properly cited and is not used for commercial purposes.

Sources of the Levantine Intermediate Water in Winter 2019

V. Taillandier¹ , F. D'Ortenzio¹ , L. Prieur¹ , P. Conan² , L. Coppola¹ , M. Cornec¹ , F. Dumas³, X. Durrieu de Madron⁴ , B. Fach⁵ , M. Fourrier¹ , M. Gentil⁴, D. Hayes⁶ , S. Husrevoglu⁵ , H. Legoff⁷, L. Le Ster^{1,8} , H. Örek⁵, T. Ozer⁹, P. M. Poulain¹⁰ , M. Pujo-Pay², M. Ribera d'Alcalà¹¹, B. Salihoglu⁵, P. Testor⁷ , D. Velaoras¹² , T. Wagener¹³ , and C. Wimart-Rousseau¹³ 

¹Sorbonne Université, CNRS, Laboratoire d'Océanographie de Villefranche (LOV), Villefranche-sur-Mer, France, ²Sorbonne Université, CNRS, Laboratoire d'Océanographie Microbienne (LOMIC), Paris, France, ³Service Hydrographique et Océanographique de la Marine (SHOM), Brest, France, ⁴CEFREM, CNRS, Université de Perpignan Via Domitia, Perpignan, France, ⁵Middle East Technical University (METU), Institute of Marine Sciences, Erdemli, Turkey, ⁶Oceanography Center, University of Cyprus, Nicosia, Cyprus, ⁷Sorbonne Université, CNRS, IRD, MNHN, Laboratoire d'Océanographie et de Climatologie (LOCEAN), Paris, France, ⁸Centre d'Etudes Biologiques de Chizé (CEBC), CNRS, Villiers-en-Bois, France, ⁹Israel Oceanographic & Limnological Research (IOLR), Haifa, Israel, ¹⁰National Institute of Oceanography and Applied Geophysics (OGS), Sgonico, Italy, ¹¹Stazione Zoologica Anton Dohrn (SZN), Villa Comunale, Italy, ¹²Hellenic Center for Marine Research (HCMR), Institute of Oceanography, Attiki, Greece, ¹³Aix Marseille Université, Université de Toulon, CNRS, IRD, MIO, Marseille, France

Abstract Climatic changes and interannual variability in the Mediterranean overturning circulation are crucially linked to dense water formation in the Levantine Sea, namely the Levantine Intermediate Water whose formation zone, comprising multiple and intermittent sources, extends over fluctuating pathways. To probe into the variability of this water formation and spreading, a unique dataset was collected during the winter of 2019 in the western Levantine Sea, via oceanographic cruises, profiling floats and a glider, at a spatio-temporal distribution suited to resolve mesoscale circulation features and intermittent convection events. This study highlights the competition between two source regions, the Cretan Sea and the Rhodes Cyclonic Gyre, to supply the Mediterranean overturning circulation in Levantine Intermediate Water. The Cretan source was estimated as the most abundant, supported by increasingly saltier water masses coming from the Levantine Sea under the pumping effect of a water deficit caused by strong western outflow toward the Ionian Sea.

Plain Language Summary The Mediterranean overturning circulation is a conveyor belt transporting salt from its easternmost areas toward the North Atlantic Ocean. To explore how the formation of dense and salty waters called the Levantine Intermediate Water fits into this circulation, the western Levantine Sea was investigated during the winter of 2019 via cruise surveys and an array of autonomous sensors. This study highlights the competition between two source regions, the southern Aegean Sea and the northwestern Levantine Sea, to supply the Mediterranean overturning circulation in Levantine Intermediate Water. In the period under study, the first region was estimated as the most abundant source. This source was supported by increasingly saltier water masses coming from the Levantine Sea, under the pumping effect of a water draught in the Aegean Sea. These observations help to nuance the complex picture of Levantine circulation patterns which are subject to large variability.

1. Introduction

The Mediterranean Sea is often considered as a miniature ocean for climatic studies (Béthoux et al., 1999; Durrieu de Madron et al., 2011; Tsimplis et al., 2006). Its semi-enclosed geometry fosters a zonal overturning circulation that connects remote areas of the easternmost Levantine Sea with the North Atlantic Ocean, in compensation for the evaporation excess over the basin (Hopkins, 1978). This open thermohaline cell sets the stratification of the whole Mediterranean Sea according to a two-layer flow (Wüst, 1961): the non-return flow of fresh waters of Atlantic origin (AW) in the surface layer, and the formation and westward spreading in the intermediate layer of salty waters, namely the Levantine Intermediate Water (LIW). This latter water mass plays a major role in the vertical exchanges of physical and biogeochemical properties as well as their arrangement and transport over the different sub-basins of the Mediterranean Sea. LIW is involved in the deep water formation processes that drive the two internal thermohaline cells in the western and eastern Mediterranean basins

(Lascaratos et al., 1999). LIW also impacts on the primary productivity of the Mediterranean Sea, regulating nutrient supply in the euphotic zone (Béthoux et al., 1998; Williams & Follows, 2003).

In the Mediterranean Sea, the vertical distribution of water mass properties is characterized by ubiquitous sub-surface salinity maxima, set at intermediate depth ranging from 250 down to 400 m, and most often associated to extrema in temperature, oxygen and nutrient concentrations (Ribera d'Alcalà et al., 2003; Kress et al., 2003; Pujo-Pay et al., 2011). These criteria are commonly used to identify the LIW and retrieve its thermohaline properties at specific locations and times. By this way, a substantial corpus has been constituted on the LIW's properties. They have been studied to determine LIW residence times in different Mediterranean sub-basins (Béthoux, 1980; Roether et al., 1998) as well as water mass fractions (Hainbucher et al., 2014; Schroeder et al., 2020). Their spatial variations at the basin scale have been analyzed to define LIW pathways and density horizons (Kovacevic et al., 2012; Malanotte-Rizzoli et al., 1997; Wüst, 1961) whereas their seasonal variations have served to characterize the volume produced (Manca et al., 2003; Özsoy et al., 1989). In addition, their long-term fluctuations have enabled inferences on climatic changes and oscillations (Bensi et al., 2016; Gačić et al., 2010; Krokos et al., 2014; Schroeder et al., 2017; Velaoras et al., 2014).

However, the significant scattering of LIW properties in the easternmost parts of the Mediterranean Sea, early pointed out by Wüst (1961), contrasts with the records of the Sicily Channel where their properties fluctuate within a remarkable narrow range (Astraldi et al., 1999; Gačić et al., 2013), even if affected by significant climatic trends (Schroeder et al., 2017). This can be explained by the existence of multiple sources of LIW: the northwestern Levantine Sea (Gertman et al., 1994; Malanotte-Rizzoli et al., 2003; Sur et al., 1992), the Cretan Sea (Georgopoulos et al., 1989; Velaoras et al., 2014), the Cilician Basin (Fach et al., 2021; Feliks, 1991), or over broader areas within anticyclones (Hecht et al., 1988; Moutin & Prieur, 2012). If LIW formation is controlled by local conditions and specific dynamical process acting on each source, LIW may also undergo further thermohaline transformations during its eastward spreading among the Levantine Sea. In other words, winter mixing activity over the Levantine Sea, preconditioned by surface saltier waters and possibly intensified by the absence of AW, can reach intermediate depths and accordingly modify “older” LIW properties. Hence, LIW type waters definitely acquire their traits (notably the sub-surface salinity maximum) when they reach the adjacent Ionian Sea.

To overcome such indetermination inside the formation zone, sources of LIW can be inferred from our knowledge of the eastern Mediterranean circulation in the surface and intermediate layers. Schematics of permanent circulation, drafted one century ago by Nielsen (1912), were detailed by Robinson et al. (1991) thanks to extensive investigations carried out during the 1980s–1990s (Malanotte-Rizzoli et al., 1996). These experimental efforts revealed highly fluctuating circulation features from seasonal to interannual scales, with respect to their occurrence, their location, and their intensity (Hecht & Gertman, 2001; Malanotte-Rizzoli et al., 1999; Theocharis et al., 1999; Özsoy et al., 1993). The northwestern Levantine Sea and the Cretan Sea were identified as two main sources adjacent to the Ionian Sea: they are dense water formation zones able to gather the other sources and to provide ultimate thermohaline transformations before ventilation of LIW type waters. Moreover, the unevenness of the circulation patterns, coupled with the non-uniformity of winter convection processes, modulate the respective activity of these sources, and trigger significant climatic variability of the Mediterranean overturning circulation (Popov, 2004; Theocharis et al., 2014; Velaoras et al., 2019). In the meantime, state-of-art Mediterranean circulation re-analyses significantly improved estimations of intermediate water mass formation sites and rates, as well as their long-term variability (Pinardi et al., 2015, 2019; Simoncelli et al., 2018; Waldman et al., 2018).

We hereby propose physical and dynamical descriptions of the western Levantine Sea during a single winter. Our analysis aims to characterize the different sources of LIW, to sketch out the nearby spreading and accumulation of LIW upstream the Ionian Sea, and to situate this seasonal snapshot within the recurrent fluctuations of the Mediterranean overturning circulation. For the reasons presented earlier, LIW type is screened with respect to its characteristics at the Sicily Channel: on density horizons of 29.05–29.10 kg m^{−3}, at intermediate depths below 200 m, with salinity larger than 38.8 (e.g., Gasparini et al., 2005; Moutin & Prieur, 2012). In other words, the study focuses on the origin of the intermediate water fraction that outflows from the Sicily Channel, so-called the LIW water type for its implication further west to the open thermohaline cell. This study is supported by extensive in-situ surveys combining dedicated oceanographic cruises, glider missions, and arrays of profiling floats. Autonomous platforms, which have considerably increased our ocean-sampling capabilities in the last decade (Roemmich et al., 2019; Testor et al., 2019), readily lend themselves to exploration of the LIW sources for clarification of the multiple formation sites and events that occur intermittently and at mesoscales (Kassiss &

Korres, 2020; Mauri et al., 2019; Menna et al., 2021). Using this unique data collection presented in Section 2, winter circulation, subduction and LIW stocks are analyzed in Section 3; the results are discussed in Section 4 in terms of formation and spreading processes, identification and respective contribution of LIW sources, and salinification trends in combination with the Mediterranean overturning circulation.

2. Data and Methods

2.1. Multiplatform Sampling and Data Coverage

An extensive investigation of the western Levantine Sea was conducted in the framework of the French program PERLE (Pelagic Ecosystem Response to dense water formation in the Levant Experiment) by means of regional-scale oceanographic cruises, and concomitant deployments of autonomous platforms (gliders, profiling floats). This observational effort was phased with the Turkish program DEKOSIM that operates recurrent field surveys over the northern Levantine Sea (Fach et al., 2021).

Four oceanographic cruises were carried out during the period May 2018–March 2019: PERLE-0 onboard *R/V Tethys II* in May 2018, PERLE-1 onboard *R/V L'Atalante* in October 2018, PERLE-2 onboard *R/V Pourquoi Pas?* in February–March 2019, and DEKOSIM onboard *R/V Billim-2* in March 2019. An array of 25 profiling floats was set up in 2018 during the PERLE-0 and PERLE-1 cruises, as components of the regional Argo and BGC-Argo programs in the Mediterranean Sea (Poulain et al., 2007; D'Ortenzio et al., 2020). A glider was deployed in December 2018–January 2019 from the facility of the University of Cyprus. Details on periods of acquisition are reported by platform in Table 1.

This multiplatform sampling strategy covered areas surrounding the Island of Crete over the three following sectors (Figure 1): (a) the Cretan Passage extending south Crete until the Ionian Sea, (b) the Cretan Sea linked with the Ionian and Levantine Seas by four deep straits of the Cretan Arc, (c) the western Levantine Sea delineated by the Anatolian coast and the eastern Cretan Arc. For the sector (c), a mesh grid of oceanographic stations (0–1,200 m) was implemented during the DEKOSIM cruise, in addition to glider transects of about 5 km resolution (0–1,000 m). For the sectors (a) and (b), a survey of ocean currents (0–1,000 m) and hydrographic transects (0–bottom) was carried out during the cruise PERLE-2. The autonomous component efficiently complemented this distribution: deployments of profiling floats that mostly occurred in June and October 2018 in the three sectors enabled large scale dispersion of the array for the winter 2019 (Figure 1, red dots). Floats were programmed to drift either at 350, 1,000, or 2,000 m depth, with a cycling period of 1–5 days (Table 1), and a maximum profiling depth of 700–2,000 m. They extended the data distribution over a period of interest from fall 2018 until summer 2019 (Figure 1). This array of profiling floats efficiently pertained the observation of the LIW formation zone by the synoptic surveys, which enabled a characterization of pre- and post-winter LIW stocks.

2.2. Data Acquisition and Processing

Thanks to these combined observational efforts, 1,847 profiles of seawater temperature and salinity have been collected between 15 October 2018 and 31 July 2019. This dataset was pooled and metrologically harmonized for the purposes of the present study.

Pressure, in-situ temperature and conductivity of seawater were measured by a CTD underwater unit (Sea Bird Electronics SBE9plus) at every station of the cruises. The accuracy of measurement of the CTD unit was 1 dbar for pressure, 0.001°C for temperature and 0.003 for salinity. Raw data were processed into quality-controlled profiles at the vertical resolution of 1 dbar as detailed in Taillandier et al. (2018).

The profiling floats and the glider were equipped with autonomous CTD sensors of high stability (Sea Bird Electronics SBE41), with an instrumental precision of 0.01 for salinity, 0.002°C for temperature and 2.4 dbar for pressure (Wong et al., 2019). Temperature and salinity profiles were collected during the ascent phase of the autonomous platforms, between at least 700 dbar and the surface, with vertical resolutions of 1–25 dbar, depending on the operational setup of the different platforms. Raw data were processed and distributed by the Coriolis Data Center after automated (real-time) quality checks (Argo, 2000). Metrological verification of autonomous CTD sensors was performed with respect to the PERLE-2 cruise's references. Salinity offsets between −0.015 and +0.020 were detected and corrected in some platforms (Table 1), which is in agreement with the expected range of such intercalibration exercises (Bordone et al., 2020).

Table 1
Composition of the Dataset, by Program Name, Platform Identification [World Meteorological Organization (WMO)], Sensor Type, Number of Profiles, Period of Acquisition, Average Cycling Period for Profiling Float, and Detected Salinity Offset

Program name	Vessel or WMO	Sensor type	# Profiles	Initial time	Final time	Cycling period (in days)	Salinity offset
PERLE-2	<i>R/V Pourquoi Pas?</i>	VM-ADCP	12,368	27-Feb-2019	16-Mar-2019		-
PERLE-2	<i>R/V Pourquoi Pas?</i>	CTD	85	27-Feb-2019	16-Mar-2019		Reference
DEKOSIM	<i>R/V Billim-2</i>	CTD	36	22-Mar-2019	27-Mar-2019		0.000
PERLE	SeaGlider 6,800,450	CTD	87	01-Jan-2019	03-Feb-2019		0.000
Argo-Italy	3,901,977	CTD	57	23-Oct-2018	30-Jul-2019	5.0	0.000
BGC-Argo	6,901,764	CTD	37	02-Nov-2018	08-Mar-2019	3.5	+0.020
BGC-Argo	6,901,772	CTD	30	07-Jan-2019	29-Jul-2019	6.7	0.000
BGC-Argo	6,901,775	CTD	49	19-Oct-2018	26-Jul-2019	5.7	+0.010
Argo-France	6,902,718	CTD	102	23-Oct-2018	29-Jul-2019	2.7	0.000
Argo-France	6,902,770	CTD	42	05-Jan-2019	29-Jul-2019	4.9	+0.010
Argo-France	6,902,845	CTD	113	24-Oct-2018	29-Jul-2019	2.4	0.000
Argo-France	6,902,846	CTD	107	24-Oct-2018	25-Jul-2019	2.6	0.000
Argo-France	6,902,847	CTD	96	24-Oct-2018	25-Jul-2019	2.8	+0.010
BGC-Argo	6,902,871	CTD	37	13-Mar-2019	05-Jul-2019	3.1	0.000
BGC-Argo	6,902,872	CTD	87	24-Oct-2018	31-Jul-2019	3.2	+0.010
BGC-Argo	6,902,873	CTD	42	13-Mar-2019	30-Jul-2019	3.3	0.000
BGC-Argo	6,902,874	CTD	86	29-Oct-2018	31-Jul-2019	3.2	0.000
BGC-Argo	6,902,898	CTD	132	16-Oct-2018	30-Jul-2019	2.2	0.000
BGC-Argo	6,902,900	CTD	51	22-Oct-2018	11-Mar-2019	2.7	+0.005
BGC-Argo	6,902,902	CTD	71	22-Oct-2018	25-Jul-2019	3.9	0.000
BGC-Argo	6,902,904	CTD	72	22-Oct-2018	31-Jul-2019	3.9	0.000
Argo-France	6,902,913	CTD	187	16-Oct-2018	29-Jul-2019	1.5	0.000
Argo-Italy	6,903,234	CTD	9	05-Jan-2019	14-Feb-2019	4.4	-0.010
Argo-Italy	6,903,244	CTD	11	04-Jan-2019	23-Feb-2019	4.5	-0.010
Argo-Italy	6,903,245	CTD	55	01-Nov-2019	29-Jul-2019	4.9	-0.010
Argo-Italy	6,903,246	CTD	56	26-Oct-2018	28-Jul-2019	4.9	-0.015
BGC-Argo	6,903,247	CTD	50	25-Nov-2018	28-Jul-2019	4.9	0.000
Argo-Italy	6,903,259	CTD	30	04-Mar-2019	27-Jul-2019	4.8	0.000
Argo-Italy	6,903,260	CTD	30	06-Mar-2019	29-Jul-2019	4.8	0.000

Ocean currents were acquired along the track of the PERLE-2 cruise by a vessel-mounted acoustic Doppler current profiler (Teledyne RD Instruments Ocean Surveyor 38 kHz), working in narrow band with a depth range of about 1,000 m and a vertical resolution of 24 m (50 bins) and a pinging period of 2 min. In winter unstratified conditions, the shallowest bin at 54 m is considered as representative of the surface layer (0–54 m). Data were processed as detailed in Taillandier et al. (2018). Moreover, a Butterworth low pass filter with a cut-off period at 20 min was applied to decrease the instrumental noise to 2 cm/s.

2.3. Diagnostics

Several diagnostics were implemented on this unique dataset in order to map geostrophic flows, characterize the water masses, assess the mixed layer properties, evaluate the stocks of LIW, and estimate the transports across three Cretan straits.

The potential temperature and potential density excess to 1,000 kg m⁻³, referenced to the sea surface (0 dbar), simplified hereinafter as “temperature” (in °C) and “density” (in kg m⁻³), were derived from *in-situ* temperature

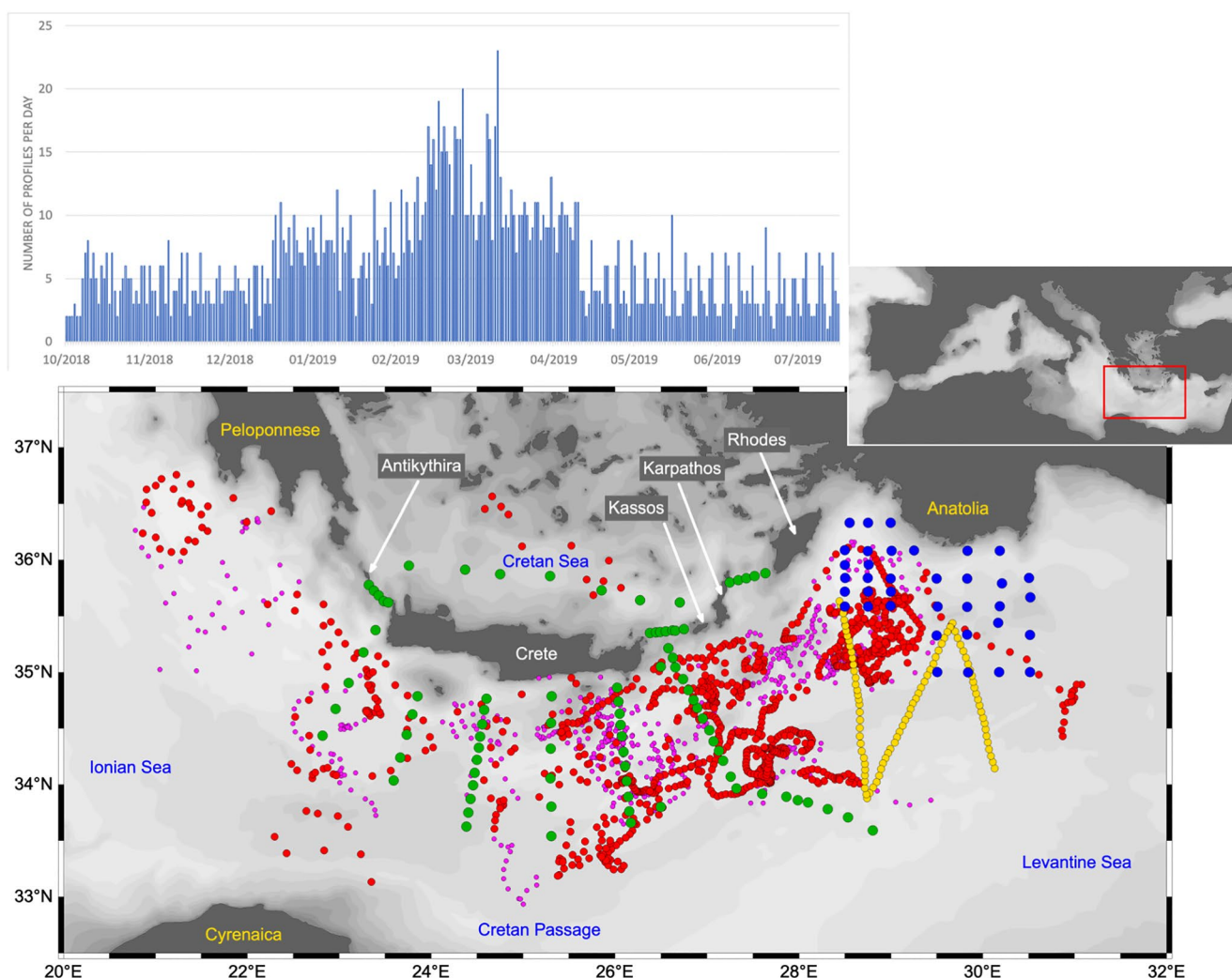


Figure 1. Distribution of the dataset over the period of study (15 October 2018–2031 July 2019). Upper panel: histogram of the number of profiles per day during. Lower panel: location of the profiles collected during the winter period (1 January 2019–15 April 2019) by the PERLE-2 cruise (85 profiles, green dots), the DEKOSIM cruise (36 profiles, blue dots), the glider (87 profiles, yellow dots), and the profiling floats (1,009 profiles, red dots). The remaining 630 profiles collected outside of that winter period are located at the purple dots. Names of the sub-basins (in blue), islands of the Cretan Arc (in white), and mainland (in yellow). Location of the region of interest (inset, red square) within the Mediterranean Sea.

and practical salinity. Considering the isopycnal 29.05 kg m^{-3} classically defined as the horizon of LIW spreading (Wüst, 1961), its depth was retrieved for every density profile. Dynamic topography (in dyn cm) relative to a reference geopotential at 500 dbar was computed as the integral of specific volume anomalies between 10 and 500 dbar. Horizontal mapping of this quantity indicates circulations tangential to the contours; gradients normal to contours allow the sizing of surface geostrophic currents (Pond & Pickard, 1983).

The depth of isopycnal 29.05 kg m^{-3} and the dynamic topography relative to 500 dbar were mapped onto winter mean horizontal fields, using the set of CTD profiles collected during the winter period (1 January–15 April 2019, Figure 1). The two fields were computed by the Data Interpolating Variational Analysis (DIVA) method (Troupin et al., 2012) with a correlation length scale of 15 km; areas with gridding errors greater than 10% are blank. The dynamic contours -39 and -42 dyn cm were extracted from the winter mean dynamic topography in order to delineate areas of specific dynamical properties, and to position ship and glider transects within the winter intermediate circulation. Sections of normal current and seawater properties were mapped into punctual two-dimensional (along-transect and vertical) fields. The fields were computed either by isopycnic gridding or weighted-average gridding, with a horizontal correlation length scale of 15 km and a vertical correlation length scale of 5 m.

The mixed layer depth was estimated from the density profiles as the depth where the residual mass content (i.e., the vertical integral of the density anomaly relative to surface) was equal to 1 kg m^{-2} (Prieur et al., 2020). This buoyancy criterium was preferred to alternative approaches such as a threshold density deviation to surface density of 0.03 kg m^{-3} (e.g., D'Ortenzio et al., 2005), in order to filter out short temporal variability of the mixed layer (notably its diurnal cycle) and reduce sensitivity to transient pycnoclines.

The mixed layer temperature and salinity were evaluated as their average value between the surface and the mixed layer depth. Water masses with thermohaline properties corresponding to the fraction of intermediate water outflowing from the Sicily Channel (salinity larger than 38.8, density within $29.05\text{--}29.10 \text{ kg m}^{-3}$), so-called the LIW type, were screened over the whole dataset. Their volumetric stock was evaluated per unit horizontal area on every profile, as the cumulated vertical extent of every seawater parcel that meets the salinity and density selection criteria.

Absolute currents measured by VM-ADCP along the track of the PERLE-2 cruise (27 February–7 March 2019, Table 1) provided estimates of average currents in the intermediate layer (78–222 m depth). Normal transports (in Sv) across three Cretan straits (0–510 m depth) were evaluated as the integral of absolute currents between the surface (bin 1 extended to 0–54 m) and 510 m (bin 20), and cumulated over the extension of the section. The average and standard deviation of water properties were evaluated in the same vertical extent using the profiles collected along the three Cretan straits during the PERLE-2 cruise (Figure 1).

3. Results

3.1. Circulation

The winter circulation (Figure 2) was marked by a sub-basin-scale structure, the Rhodes Cyclonic Gyre (RCG) that covered the northwestern Levantine Sea ($26^{\circ}30'\text{E}\text{--}30^{\circ}\text{E}$), and several mesoscale features that developed in chains of eddies across the Cretan Passage. All these features, interconnected by intense geostrophic jets, were equally documented by three different observations: (a) the absolute currents, (b) the topography of the isopycnal 29.05 kg m^{-3} (shallow in the cyclones, deep in the anticyclones), and (c) the geostrophic jets (tightening of dynamic contours). They are in overall agreement in amplitude and direction.

The site of isopycnal outcrops delineated a convection zone extending on the center of the RCG over 250 km from northeast to southwest. At its northern and eastern rims, the Asia Minor Current (AMC) flowed along the Anatolian coast as far south as the entrance of the Cretan Passage. This geostrophic jet meandered, detrained in small-scale eddies, and partly entered the Cretan Sea. A second bifurcation occurred downstream in the presence of an anticyclonic eddy (AE1 centered at $26^{\circ}45'\text{E}$). One branch was retroflected eastward along 34°N , until another anticyclonic eddy (AE4 centered at $28^{\circ}30'\text{E}$), to compose the southeastern rim of the RCG. The other branch was guided across the Cretan Passage, veered south around a two-lobe anticyclonic system (AE2 centered at $25^{\circ}45'\text{E}$ and AE3 centered at 25°E), and progressively weakened downstream into small recirculation cells (centered at $25^{\circ}15'\text{E}$, $24^{\circ}30'\text{E}$, $23^{\circ}45'\text{E}$). The Cretan Cyclone (CC centered at 23°E) extended over 150 km in the western Cretan Passage. It was surrounded in the northwest by the Pelops Anticyclone (PA centered at $21^{\circ}30'\text{E}$) offshore the Peloponnese, and in the southwest by a partially documented geostrophic structure offshore the Cyrenaican Coast.

Water exchanges with the Cretan Sea were characterized by punctual transects across the Cretan straits, carried out at the beginning and at the end of the PERLE-2 cruise (Table 2). The bifurcation of the AMC into the Cretan Sea was documented by two veins of current, extending in the upper 300 m with amplitudes up to 50 cm/s, and flowing in geostrophic balance with isopycnals along the western flanks of the straits (Figures 3b and 3c). These inflows partly recirculated into local cyclonic cells at the eastern side of the sections. The associated transport was estimated at 1.0–1.2 Sv per strait (Table 2). On the other hand, the transect across the western strait showed an intense outflowing current (25–50 cm/s), which extends in the upper 400 m over the entire section (Figure 3a); the associated transport was estimated at 3.3 Sv (Table 2). This outflow was most likely balanced by the successive AMC inflows across the eastern straits with respect to volume conservation of the Cretan Sea over timescales of a month. Inferred from this hypothesis, the transport across the northeasternmost strait along the Anatolian coast (undocumented) would have reached 1.1 Sv. Moreover, the AMC water inflow across the eastern straits was warmer (by $>1^{\circ}\text{C}$), fresher (by 0.13) and less dense (by 0.17 kg m^{-3}) than the outflow across western strait ($39.12/15.40^{\circ}\text{C}/29.07 \text{ kg m}^{-3}$, Table 2), resulting from intense thermohaline transformations in the Cretan Sea.

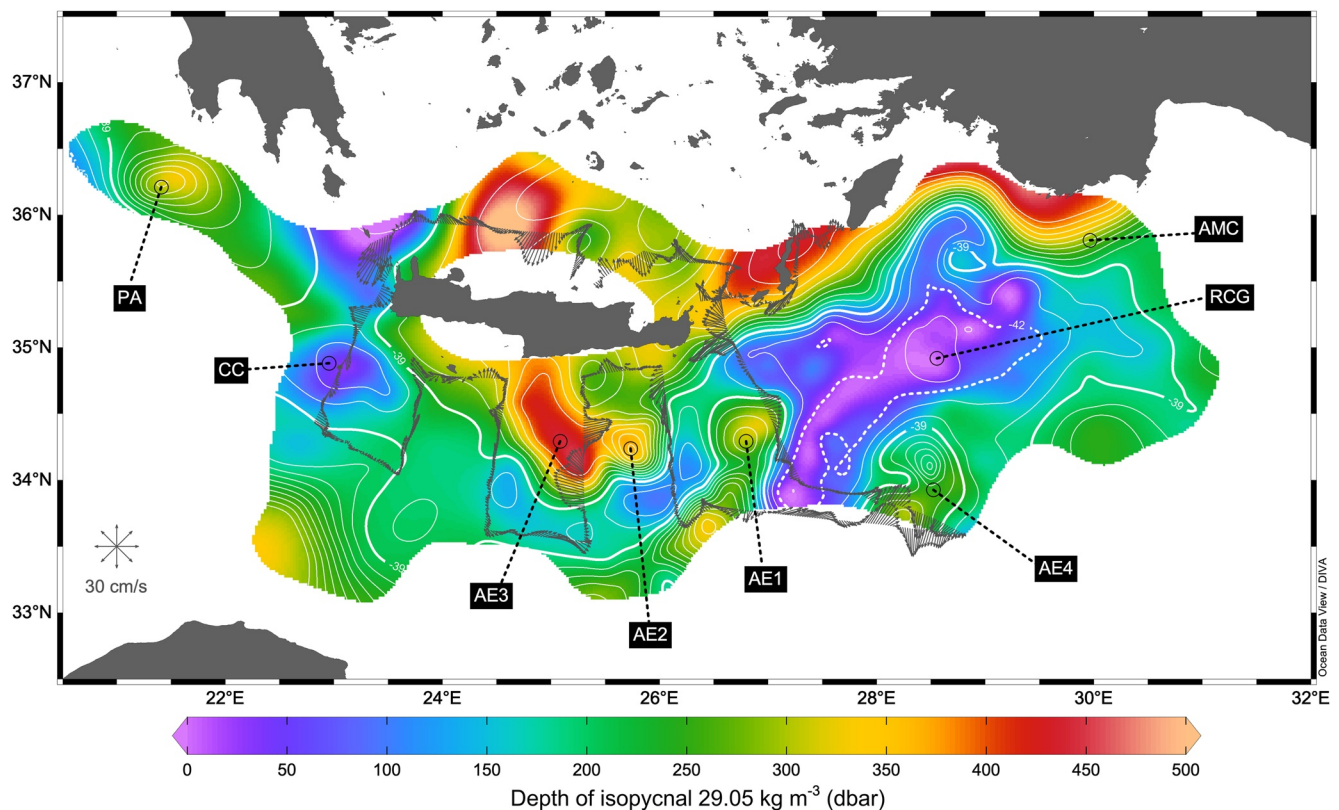


Figure 2. Depth of isopycnal 29.05 kg m^{-3} mapped for the time interval 1 January–15 April 2019 (color-coded by depth of isopycnal). Winter mean dynamic topography relative to 500 dbar (superimposed white lines, interval 1 dyn cm, thick solid line -39 dyn cm, thick dotted line -42 dyn cm). Absolute currents measured along the ship track in the intermediate layer during the PERLE-2 cruise (78–222 m depth, gray arrows, in cm/s, compass rose 30 cm/s). Locations of the dynamical structures: Pelops Anticyclone (PA), Cretan Cyclone (CC), anticyclonic eddies (AEs), Rhodes Cyclonic Gyre (RCG), and Asia Minor Current (AMC).

3.2. Subduction

Focusing on the convection zone of the RCG (delineated by the dynamic contour -42 dyn cm, Figure 4), the progressive deepening of the mixed layer started in late November 2018 and reached 100 m depth at the end of December. This preconditioning period was matched with the cooling and the freshening of surface waters. The thermostat of 15°C was reached in January and remained until March. This period of convection was marked by two mixing events: one in mid-January down to 400 m and one at the end of February down to

Table 2

Water and Flow Properties Across the Main Cretan Straits (0–510 m) Collected During the PERLE-2 Cruise, Following the Three Sections Presented in Figure 3

	Western Cretan strait (Antikythira-Crete)	Southeastern Cretan strait (Crete-Kassos)	Northeastern Cretan strait (Karpathos-Rhodes)
Date of acquisition	28 February 2019	12 March 2019	13 March 2019
Lateral/vertical extents	30 km/0–510 m	35 km/0–510 m	37 km/0–510 m
Temperature ($^\circ\text{C}$)	15.40 (0.15)	16.49 (0.21)	16.76 (0.33)
Salinity	39.12 (0.02)	39.25 (0.03)	39.26 (0.05)
Density (kg m^{-3})	29.07 (0.02)	28.90 (0.02)	28.85 (0.04)
Normal transport (Sv)	3.3	1.2	1.0
Flow direction (to)	SW (outflow)	N (inflow)	N (inflow)

Note. Thermohaline properties reported by average (standard deviation) values over section extents. Note that the northeasternmost strait between the Island of Rhodes and the Anatolian coast has not been documented.

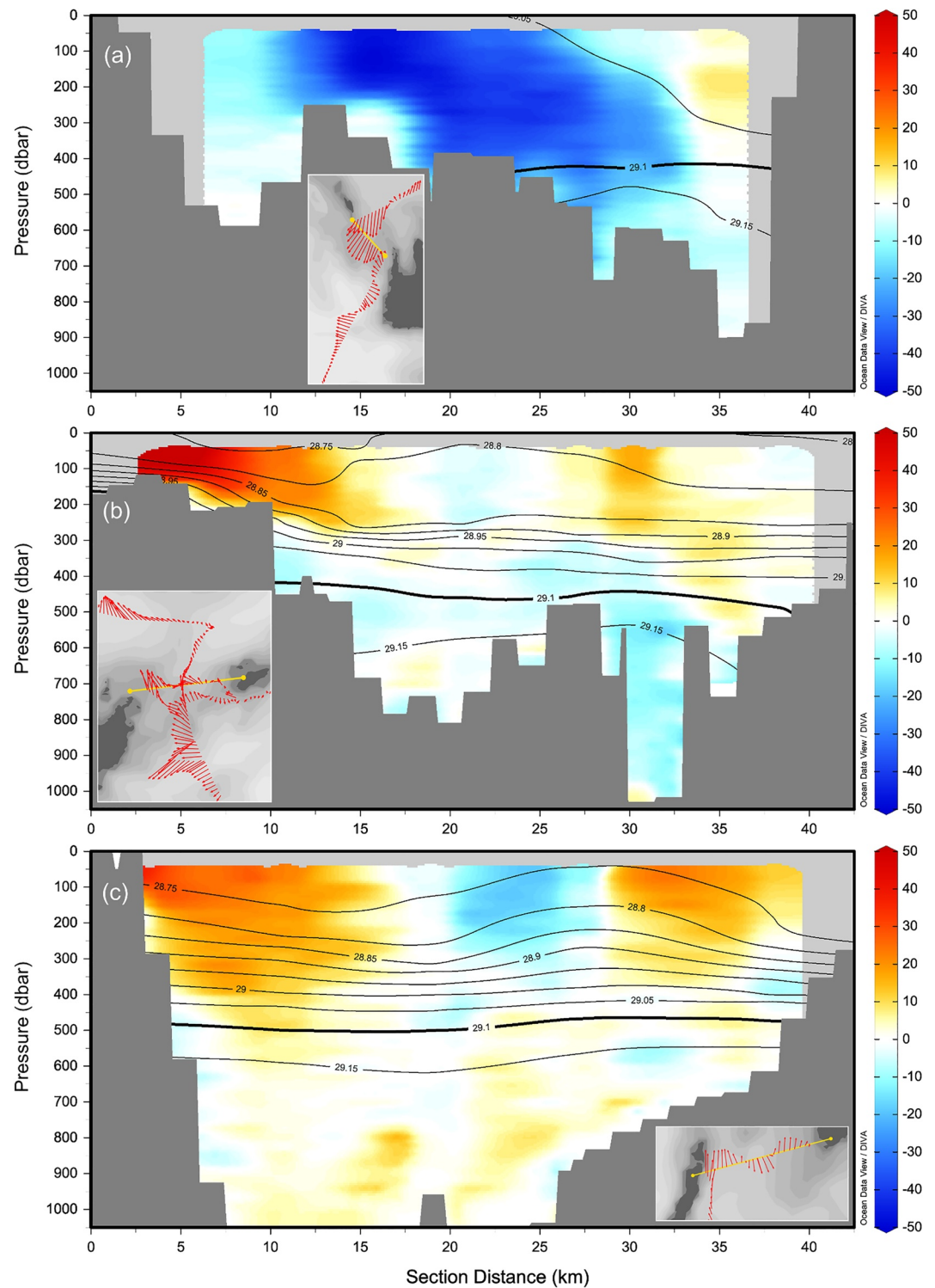


Figure 3. Sections across three Cretan straits collected during the PERLE-2 cruise. Absolute current normal to the section (color-coded, in cm s^{-1} , positive values toward the Cretan Sea) and isopycnals (black lines, in kg m^{-3} , every 0.05 kg m^{-3} , thick line 29.10 kg m^{-3}). (a) western strait (Antikythira-Crete) on 28 February 2019, (b) southeastern strait (Crete-Kassos) on 12 March 2019, (c) northeastern strait (Karpathos-Rhodes) on 13 March 2019. Insets: location of the sections (yellow lines) and details of the flow in the intermediate layer (78–222 m depth, unscaled, extracted from Figure 2). General view of the straits along the Cretan Arc indicated in Figure 1.

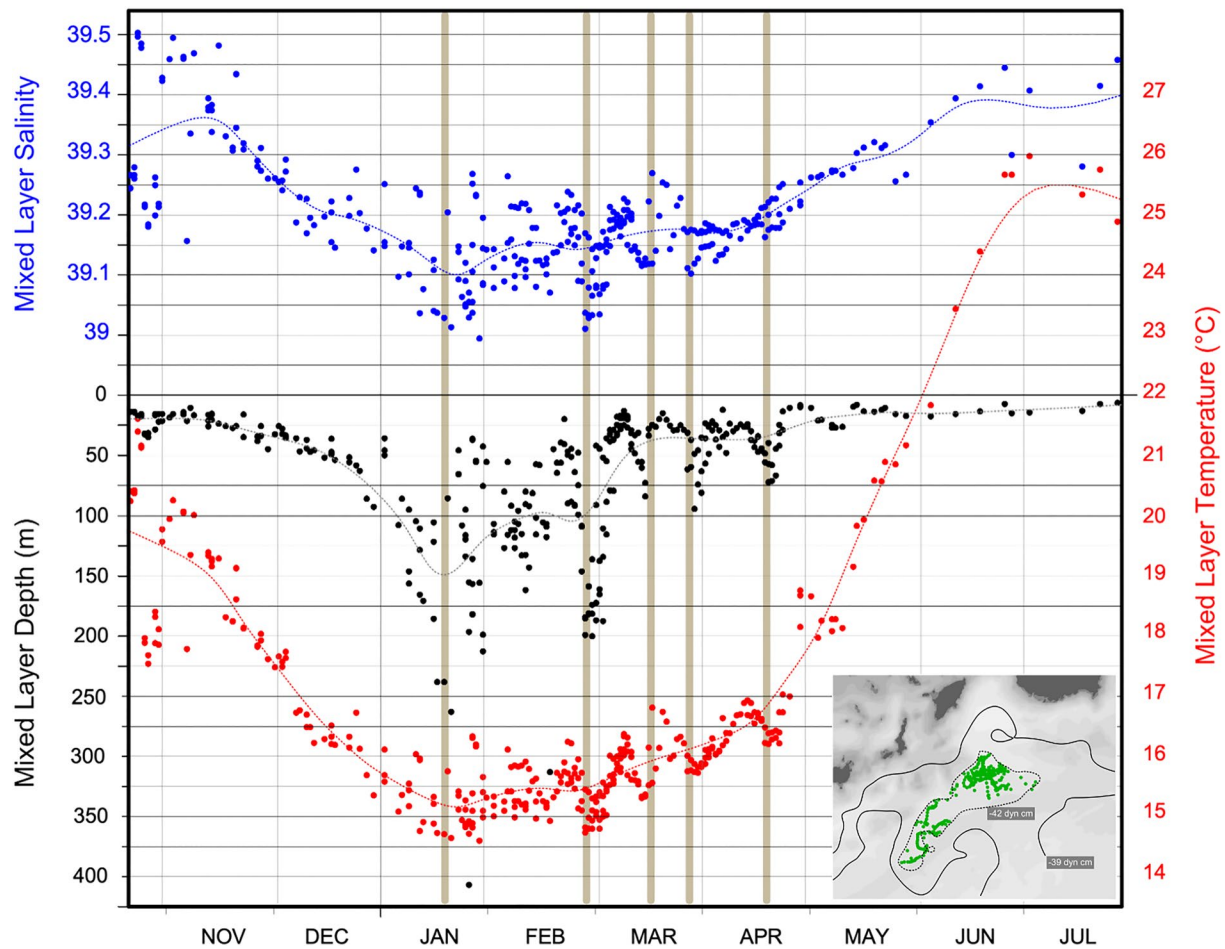


Figure 4. Depth (black), salinity (blue) and temperature (red) of the surface mixed layer inside the convection zone of the RCG delineated by the dynamic contour -42 dyn cm. Time interval: 15 October 2018–2031 July 2019. Medium-term (30-day window) fluctuations are represented by dotted lines. Mixing events indicated by vertical brown lines. Inset: representative dynamic contours (gray lines) and the 336 selected CTD profiles (green dots).

200 m. The surface waters had similar properties, $39.03/14.71^{\circ}\text{C}/29.16 \text{ kg m}^{-3}$ in salinity/temperature/density, for the two mixing events. An abrupt shallowing of the mixed layer (up to 25 m depth) occurred during the first week of March. However, convection remained active with three consecutive mixing events down to 75 m. Contrary to the previous events, the surface waters had increasingly lighter but saltier thermohaline properties: in mid-March $39.13/15.35^{\circ}\text{C}/29.08 \text{ kg m}^{-3}$, at the end of March $39.17/15.87^{\circ}\text{C}/28.99 \text{ kg m}^{-3}$, in mid-April $39.22/16.38^{\circ}\text{C}/28.91 \text{ kg m}^{-3}$. The heating period then started in mid-March, with continuous increases of surface temperature and salinity, to reach surface properties higher than 25.5°C and 39.4 in summer.

A glider section across the convection zone was carried out during the first mixing event in mid-January (Figure 5a). The mixed patch was about 50 km width, actually delineated by the dynamic contour -42 dyn cm; it was composed of dense and cold waters (larger than 29.10 kg m^{-3}) in a vertical extent of 150 m. Small scale convective chimneys of larger vertical extent (up to 400 m) but less than 10 km width were observed in the center and in the edge of the mixed patch. The area surrounding the mixed patch was composed of lighter ($29\text{--}29.05 \text{ kg m}^{-3}$) but saltier (39.2) waters in the upper 200 m depth. Salty lobes were observed at the flanks of this patch, sinking along isopycnals $29.05\text{--}29.10 \text{ kg m}^{-3}$. Further outside, a second surrounding patch of even lighter (lower than 29 kg m^{-3}) and saltier (39.3) waters was clearly delineated by the dynamic contour -39 dyn cm.

The mixed patch was also sampled in its southwestern part during the beginning of March (Figure 5b). At that time, the retreat of the mixed layer occurred and left a salty surface layer of about 30 m depth. Further north in the same section, the AMC was crossed at its bifurcation with the southeastern Cretan strait; at this location, the

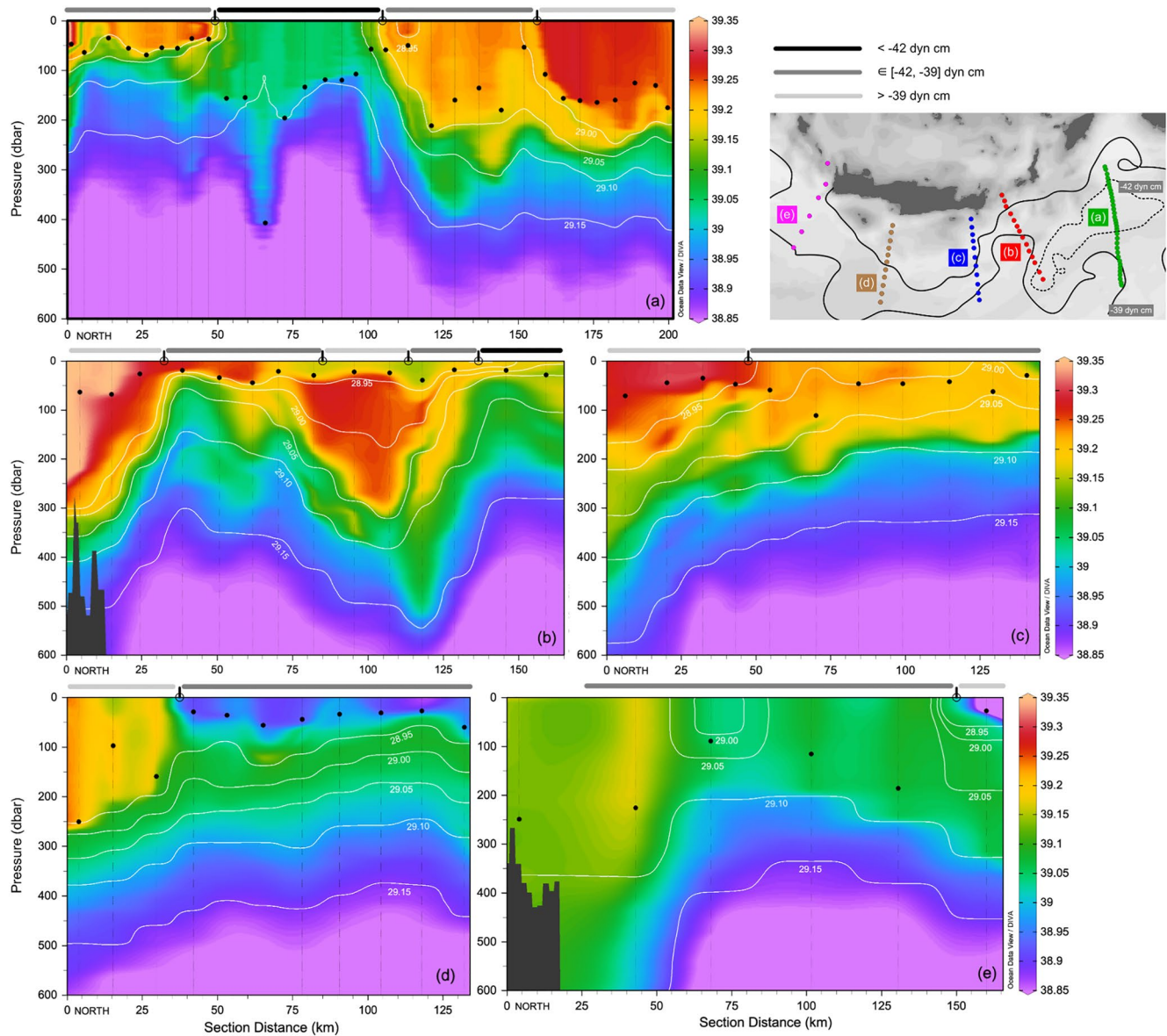


Figure 5. Salinity sections across the northwestern Levantine Sea and the northeastern Cretan Passage during the winter of 2019. Superimposed, mixed layer depth (black dots at every profile) and isopycnals (white lines, in kg m^{-3} , every 0.05 kg m^{-3}). (a) Glider transect of 19–30 January 2019 (about 5 km resolution). (b) PERLE-2 cruise transect of 11–12 March 2019 (10–15 km resolution). (c) PERLE-2 cruise transect of 6–7 March (15 km resolution). (d) PERLE-2 cruise transect of 3–4 March (15 km resolution). (e) PERLE-2 cruise transect of 1–2 March (25 km resolution). The three areas delineated by the dynamic contours -42 and -39 dyn cm are indicated on top of each panel in light, moderate and dark gray. Inset: location of the four sections and of the associated profiles (colored dots); dynamic contours -42 and -39 dyn cm (black lines).

geostrophic jet had a vertical extent of 300 m. In the transition zone with AE1 between the dynamic contours -39 and -42 dyn cm, salty waters were observed sinking isopycnally and interleaving with AE1 core waters. The two contemporary sections collected in the Cretan Passage showed the remnant AMC, with a reduced vertical extent (Figures 5c and 5d). Isopycnals 29.05 – 29.10 kg m^{-3} progressively deepened westwards, shaping an intermediate layer of salty water covered by fresher waters in the surface. The section along 23°E documented, at coarser resolution, the spreading of the Cretan water outflow into the western Cretan Passage during the beginning of March (Figure 5e). The water mass flowed on the density horizons 29.05 – 29.10 kg m^{-3} ; one part was dragged by the CC sinking along its southern flank below a fresher and lighter surface layer.

Overall, effective subduction of LIW type waters could be inferred from the observation of salty lobes, most likely originating from the upper waters around the mixed patch and cooled down during winter, hence sinking

along isopycnals $29.05\text{--}29.10\text{ kg m}^{-3}$. Subduction resulted from these downward motions, collectively triggered along the edges of the mixed patch, still active near the mixed patch with a progressive decay further west in the Cretan Passage, and reactivated in the flanks of the CC.

3.3. Stocks

Water masses of thermohaline properties matching with the LIW type (salinity larger than 38.8, density within $29.05\text{--}29.10\text{ kg m}^{-3}$) were screened over the region of interest during the period January–July. Their vertical extent at every profile made stock assessments per unit horizontal area. Stocks in the upper layer, subject to convection, subduction or restratification, could still not be considered as LIW (Figure 6a); whereas stocks in the intermediate layer, most likely not subject anymore to ventilation, were made up of LIW (Figure 6b). The choice of a threshold at 200 m depth was motivated by the characteristics of the LIW outflow at the Sicily Channel (see Introduction). On the basis of this vertical partition, the region of interest could be divided into five contrasted sectors (delineated in Figure 6): areas of subduction (sector A), areas of upwelling (sector C), and areas of LIW accumulation in the Cretan Passage (sector B), offshore the Peloponnese (sector D) and in the Cretan Sea (sector E). The central area of the RCG was mostly depleted in LIW. The LIW stocks became increasingly larger moving away from the convection zone while dense salty waters extending there on a thick surface layer (43 m in average) subducted in the periphery. Upper layers became progressively depleted, apart from the CC that locally favored upwelling. In the Cretan Passage, accumulated LIW reached an average thickness of 56 m. Moreover, the largest LIW stocks were found in the Cretan Sea (average thickness of 112 m) and in the Ionian Sea offshore the Peloponnese (average thickness of 148 m), under the caveat of coarser sampling resolution (at least one profile every 2 days in sectors A, B, C, and one profile every 5 days in sector D).

If the geographical distribution of stocks (Figure 6) remained valid at any time of the period, there were also seasonal trends extracted from the high scattering of punctual values applying a moving average filter on a 30-day window (Figure 7). In the sector A, average stocks progressively increased from 40 m in mid-October up to 75 m at the end of February. This augmentation occurred initially in the upper layer, and then, the intermediate layer of the RCG periphery was supplied under the effect of subduction. Moderate convection in the center of RCG temporarily inflected this overall increase during January with a plateau at 55 m. Meanwhile in the Cretan Passage (sectors B and C), average stocks remained constant at 60 m until an abrupt increase at 85 m during February–March, corresponding to the westwards spreading of subducted waters. The same pattern occurred in the sector D: the large increase from March (110 m) until June (160 m) was triggered to the strong outflow at the western Cretan strait. The LIW stocks almost recovered their pre-winter levels in the sectors A and D after a 2-month decrease, whereas they remained at higher levels in the Cretan Passage.

The evolution of hydrological properties during the stratification period (1 April–31 July) allowed identification of the different LIW types present in each sector as they became confined, either by subduction or retreat below lighter waters that intruded or formed during springtime. Considering the sector A (Figure 8a), thermohaline properties evolved to progressively warmer and saltier values, shaping a large beam of winter surface waters capped by direct heating either in the central area of the RCG or in its periphery. Subsurface salinity maxima associated to subducted LIW (along the isopycnal 29.08 kg m^{-3}) were transient as they appeared only in early spring. Instead, the sub-surface maxima associated to the AMC core waters (along the isopycnal 28.75 kg m^{-3}) remained and became saltier during the season.

In the sector B, springtime stratification resulted from heating (prevailing evaporation) and AW intrusions (Figure 8b). The beam of evolution identified in the RCG has changed shape with saltier values in the density classes $28.75\text{--}29.05\text{ kg m}^{-3}$. Subsurface salinity maxima associated to AEs core waters appeared along the isopycnals $28.9\text{--}29\text{ kg m}^{-3}$. The density class $29\text{--}29.1\text{ kg m}^{-3}$ was also populated by fresher waters than in the sector A. This shift, even accentuated in the sector C (Figure 8c), was associated to AW intrusions around the CC as northward detrainments at the confluence with the AE3: the presence of AW during winter avoided the ventilation of LIW upwelled by the CC, and allowed to identify a slightly fresher LIW characterized by a sub-surface salinity maximum at 39.06. In the sector D, AW intrusions occurred latter in the season (only during summer, Figure 8d). Springtime stratification was thus primarily organized by heating, upon Ionian LIW reservoirs or above Cretan water outflows.

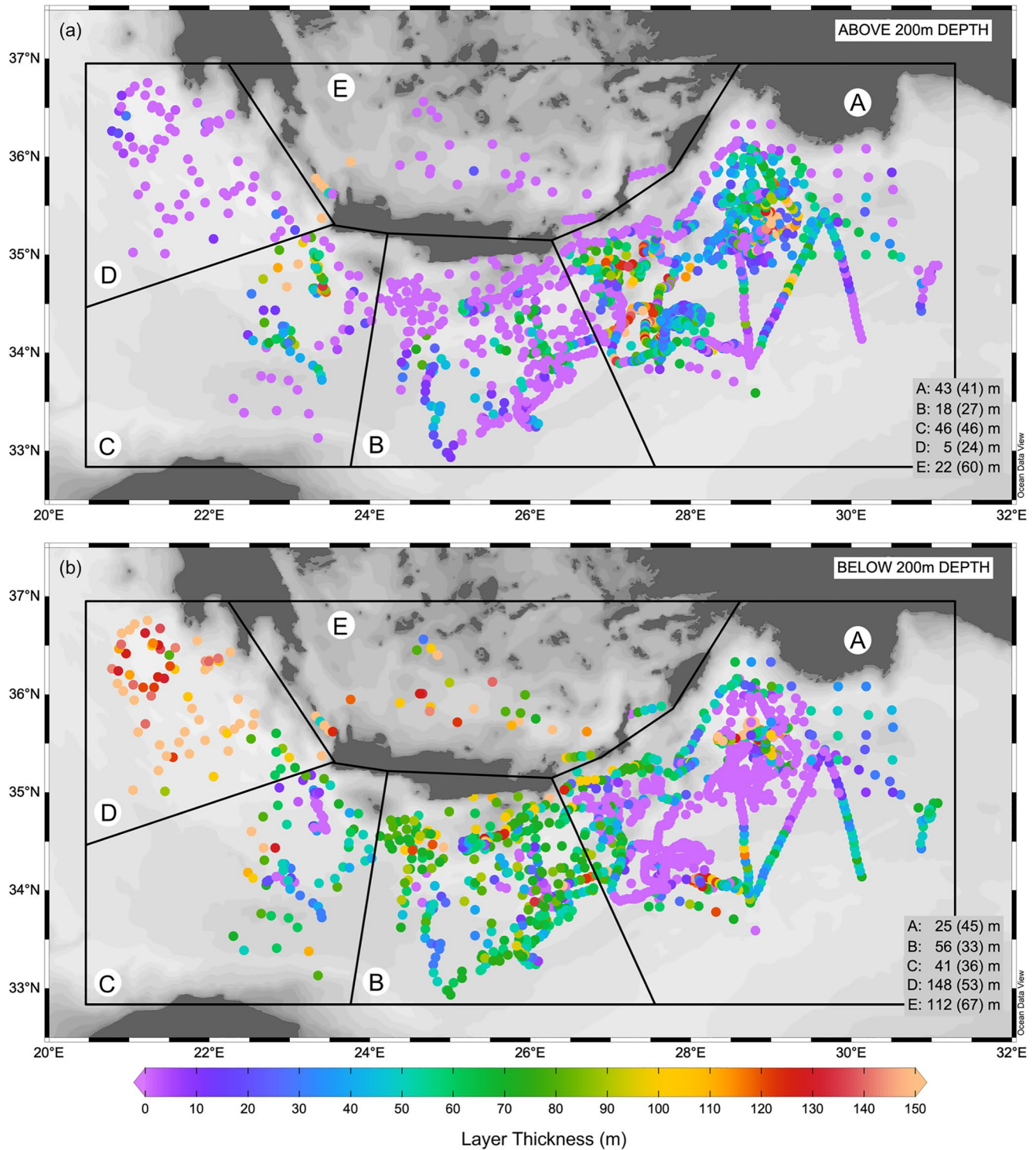


Figure 6. Layer thickness of water masses within the density class $29.05\text{--}29.10\text{ kg m}^{-3}$ with salinity larger than 38.8, estimated on every profile of the dataset collected during the period 1 January–31 July 2019. Upper panel: stocks above 200 m depth possibly subject to subduction. Lower panel: stocks below 200 m depth of LIW type. Insets: average values and associated standard deviation by sector.

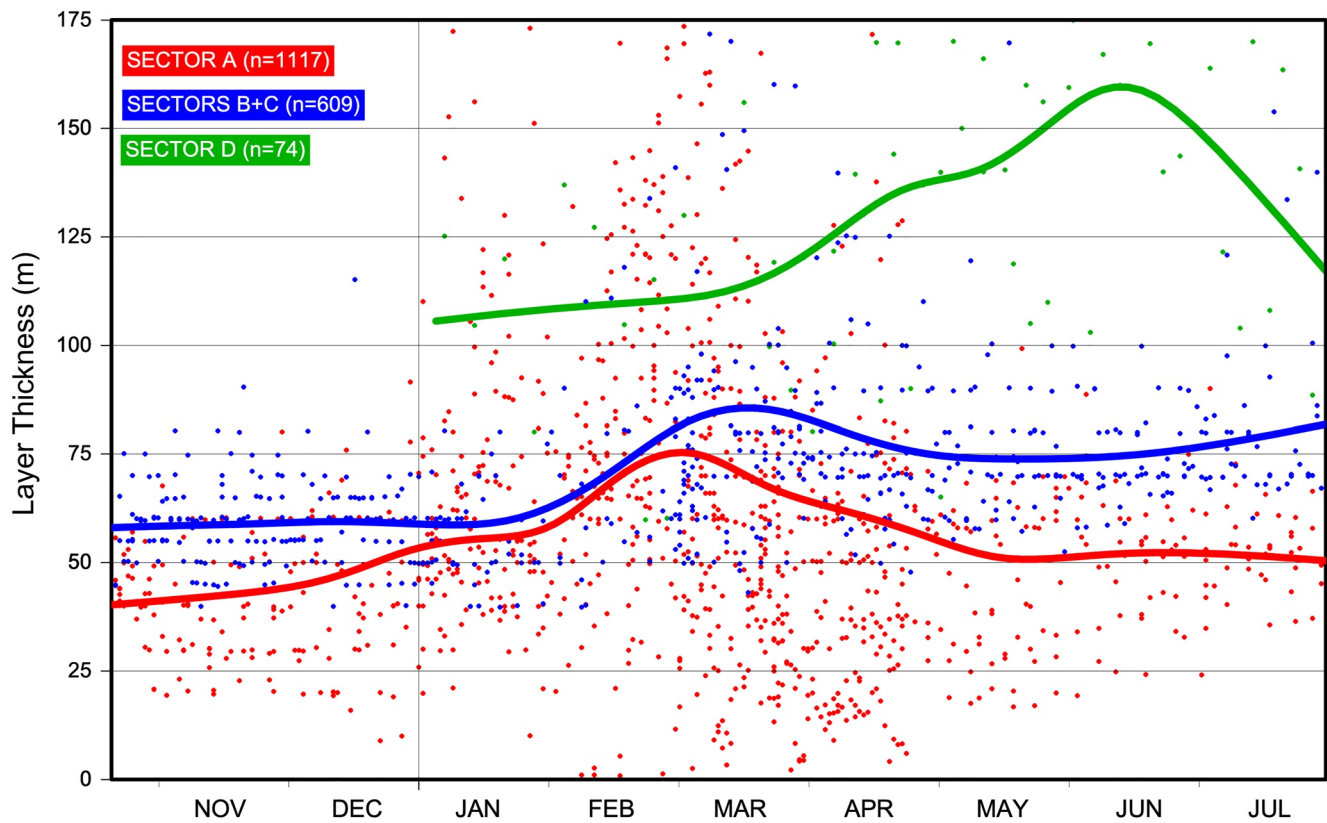


Figure 7. Layer thickness of water masses within the density class $29.05\text{--}29.10\text{ kg m}^{-3}$, estimated on every profile of the dataset without vertical partition. Scattered values and medium-term (30-day window) fluctuations for the sector A (in red), the sectors B and C (in blue), and the sector D (in green). Sectors delineated in Figure 6.

4. Discussion

4.1. Formation and Spreading

The different hydrodynamical features, reported from the analysis of the winter 2019 situation and gathered in a schematic circulation of the western Levantine Sea (Figure 9), are now discussed in the light of LIW formation and spreading processes.

Let us first consider the distinct formation processes for LIW and deep waters. The cyclonic aspect of the north-western Levantine circulation is most likely controlled by the AMC. This geostrophic jet flows along the Anatolian coast, the eastern Cretan Arc, and progressively veers northeastward at the entrance of the Cretan Passage, overall designing the RCG rim current (Figure 2). Similar Mediterranean cyclonic gyres have been quantitatively studied, in the Gulf of Lions (Testor et al., 2018), the Ligurian Sea (Prieur et al., 2020), in the Adriatic Sea (Poulain, 2001), which bears a resemblance to winter intensification of the RCG (Marullo et al., 2003) and the seasonal enhancement of vertical circulations. In the present observation, the AMC flows further west, its thickness reaches 300 m depth, its isopycnals sharpen and outcrop along a density front separating the light and salty waters of the current with denser central waters, overall designing a doming structure (Figures 2 and 5). Meanwhile, convection sporadically occurs in the central area of the RCG, opening a large mixed patch and triggering the formation of deep waters denser than LIW (as observed during January and February, Figures 4 and 8a). This is a dominant process in the other Mediterranean cyclonic gyres; however such formation events can occur intermittently in the RCG (e.g., Gertman et al., 1994; Kubin et al., 2019; Sur et al., 1992). The reported glider transect (Figure 5a) crossed one sub-mesoscale coherent vortex, formed among the mixed patch during a short-term event of moderate convection, as previously described in similar Mediterranean cyclonic gyres (Bosse et al., 2016; Testor et al., 2018).

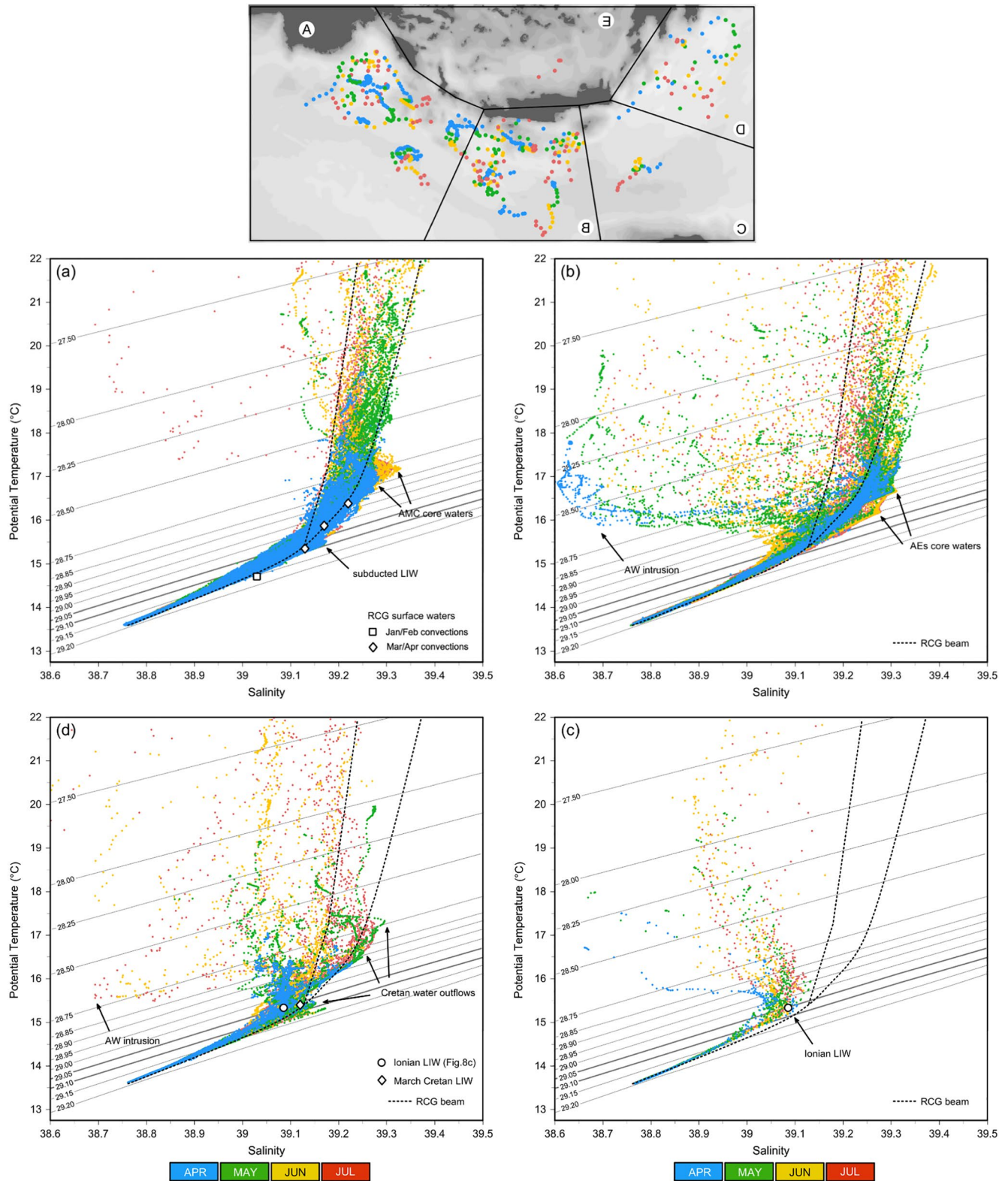


Figure 8. Temperature-salinity diagrams by sector. (a): sector A, (b): sector B, (c): sector C, (d): sector D. Sectors delineated in Figure 6. The period, from 1 April until 31 July 2019, is indicated by color (sector E undocumented during this period). Inset: profiles locations per month.

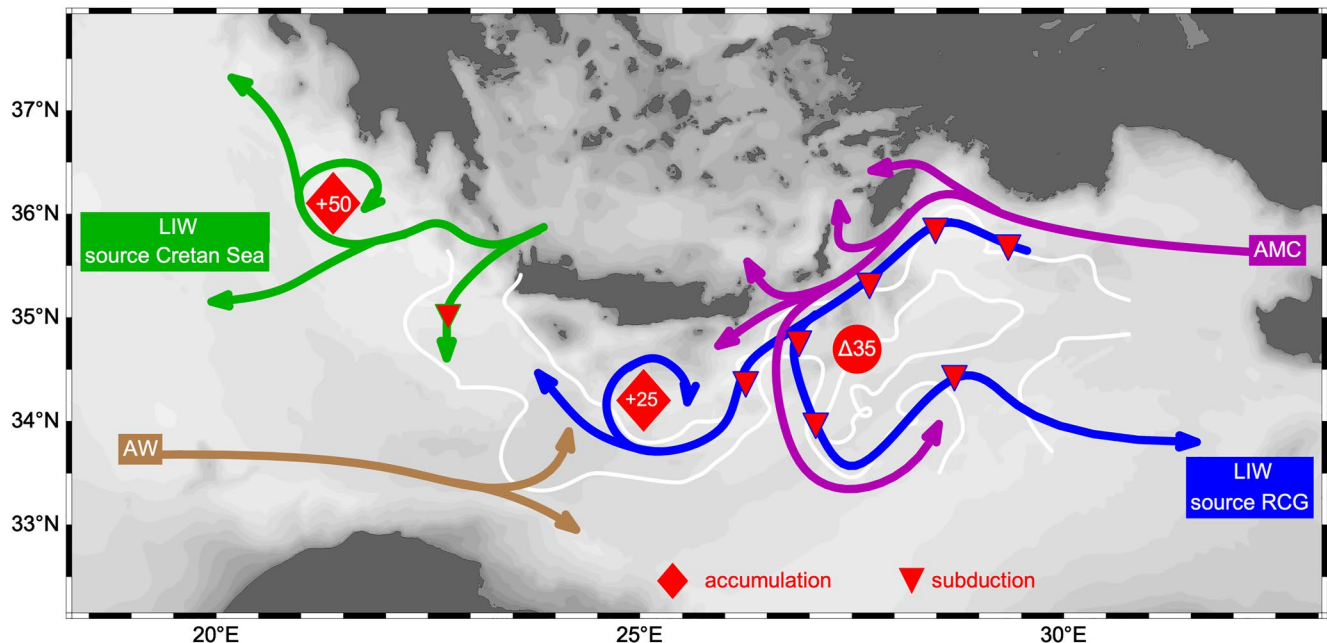


Figure 9. Schematic regional circulation inferred from multi-platform surveys between 15 October 2018 and 31 July 2019. The light and salty waters supplied by the AMC were transformed into LIW from two sources: the RCG and the Cretan Sea. AW was not observed in the two source regions. Part of LIW resulting from subduction in the periphery of the RCG was accumulated in the Cretan Passage. LIW resulting from the Cretan outflow was accumulated offshore the Peloponnese. Wintertime variations of LIW stocks indicated in meter per unit horizontal area. Locations of subduction (red triangles) and accumulation (red diamonds), dynamic contours -42 and -39 dyn cm (white lines).

On the other hand, it is important to stress that LIW type waters are formed in the periphery of the RCG (e.g., Özsoy et al., 1989). Our results show lighter but saltier waters present in the surface mixed layer at the edges of the mixed patch, and lobes of such waters isopycnally sinking at intermediate depth below the AMC (Figure 5). Submesoscale symmetric instability could be a candidate process to explain the effective subduction of LIW type water in the RCG. It has been shown in similar Mediterranean cyclonic gyres that such process can induce intense vertical movements on the dense side of fronts surrounding deep convection areas and overturn water along isopycnals within cross-frontal slanted cells (Bosse et al., 2021). Furthermore, vorticity dynamics predict that Mediterranean boundary currents, including AMC, experience strong net sinking, with a direct contribution to intermediate and deep-water formation (Pinardi et al., 2019; Waldman et al., 2018).

Considering now LIW spreading processes, our results show that LIW is channeled out of the RCG following the pathways of its rim current, which is in agreement with the previous descriptions (e.g., Malanotte-Rizzoli et al., 2003). Indeed, the AMC is found in continuity with the geostrophic jets downstream, interconnecting mesoscale eddies in the Cretan Passage (Figure 2). Remnant AMC core waters and LIW are accumulated there (Figure 6b). The flow is dispersed by AEs, inducing substantial recirculations and local confinements in salty water reservoirs (as also described by, e.g., Kress et al., 2003; Popov, 2004; Menna et al., 2021). Besides, an important structure of the region, the Ierapetra anticyclone does not clearly appear as a warm and salty surface water core in southeast Crete, although it was present during autumn 2018 (not shown). It may have evolved in AE1 or AE3 (Figure 2), with a smaller radius and larger depth extent, which is in agreement with the structural evolutions observed during the lifetime of the eddy (Ioannou et al., 2017; Popov, 2004). These changes notably favor water confinements at intermediate levels and participate to the accumulation of LIW in the Cretan Passage.

Our results show that a significant part of the RCG rim flow intrudes into the Cretan Sea, in balance to the water deficit resulting from the intense western outflow toward the Ionian Sea. Such salty waters can settle the preconditioning conditions to active convection, as winter mixing down to intermediate depths is recurrently observed in the Cretan Sea (e.g., Georgopoulos et al., 1989; Velaoras et al., 2014, 2017). As a result for the winter 2019 situation, LIW type waters are formed there and channeled out across the western Cretan strait, directly flowing out to the Ionian Sea. The transports across the Cretan straits estimated in this study (about 1 Sv at each eastern strait, 3 Sv at the western strait) remain in agreement with the wintertime report of Kontoyiannis et al. (1999).

4.2. Multiple Sources

The present analysis of winter 2019 identifies two source regions (i.e., regions where LIW type waters are formed): the RCG and the Cretan Sea (Figure 9). Both regions are supplied by the AMC flow: light and salty waters are transported from the eastern Levantine Sea, where salt reservoirs are maintained by strong summertime evaporation and the absence of river runoff. First, AMC waters supply the upper layer of the RCG, where they are cooled down during winter, and subduct in the periphery of the convection zone. This thermohaline transformation has provided in 2019 amounts of LIW of about 35 m per unit horizontal area (Figure 7). Second, AMC waters also intrude into the Cretan Sea. They are transformed during winter and supply an outflow of LIW type waters into the Ionian Sea, estimated at 3.3 Sv on 28 February 2019 (Table 2). Extrapolated over 1 month, this transport would represent a 100 m layer thickness extending over an area of about $3.3 \text{ Sv} \times 30 \text{ days}/100 \text{ m} = 10^5 \text{ km}^2$ which is approximately sizable as the area of the Cretan Sea, thus leading qualitatively to amounts of LIW formed in the Cretan Sea of about 100 m per unit horizontal area.

Overall, the Cretan source is about three times more abundant than the RCG source. The occurrence of the large outflow from the Cretan Sea appears to be linked to the weakening of LIW pathway across the Cretan Passage. The Cretan source acts as a water draught for the salt reservoirs carried out by the AMC and the RCG source gets consequently mitigated. Moreover, pre-winter stocks are relatively low in the Cretan Passage (50 m per unit horizontal area, sectors B + C, Figure 7) compared to the ones in the eastern Ionian Sea (110 m per unit horizontal area, sector D, Figure 7). Their increase during winter by new LIW represents about 50% of the pre-winter stocks. The post-winter stocks remain stable in the Cretan Passage, but the LIW reservoir of the eastern Ionian Sea is progressively depleted in order to supply the return branch of the open thermohaline circulation. In this schematic view, the PA (Figure 2) acts as a buffer structure that plays a regulating role between newly formed LIW inflow during wintertime, and the all-year LIW supply to the overturning circulation. This hypothesis is reinforced by the observation of the Pelops anticyclone as a remnant structure over the last decade (Menna et al., 2021).

In this wider perspective of the Mediterranean overturning circulation, the incoming flow composed of AW does apparently not intrude in either the RCG or the Cretan Sea. In consequence, the activity of the two sources is not mitigated by AW during the winter 2019. Some AW intrusions are detected in the western and northern parts of the Cretan Passage (Figure 8), but in lack of full coverage, the present dataset did not provide any insight of the AW flowing farther east across the southern part of the Cretan Passage, or recirculating inside the Ionian Sea. Further investigations will be necessary to evaluate the erosion of this water mass along its path toward the Levantine Sea and link the relative contribution of LIW sources with the reversal of the upper Ionian circulation (Velaoras et al., 2014).

Thanks to the extensive investigations carried out during the 1980s–1990s, observational evidence and process understanding led to identification of the different features of the Levantine circulation, their origins and their variability from seasonal to interannual scales (Hecht & Gertman, 2001; Malanotte-Rizzoli et al., 1999; Özsoy et al., 1993; Theocharis et al., 1999). These landmark findings offer a precious context for the present report. The winter 2019 circulation bears a resemblance with types of circulation characterized by a large-scale frontal zone around the RCG, the northern part of the Cretan Passage (north 34°N) and the Cretan Sea (Özsoy et al., 1989 and Figure 4 therein; Theocharis et al., 1993 and Figure 14 therein). When described for the first time, such large-scale situation was presented as unusual and thought to be probably connected with the Eastern Mediterranean Transient (Malanotte-Rizzoli et al., 1999): the enhanced salinification of the western Levantine Sea drove active convection that winter (Georgopoulos et al., 1989; Gertman et al., 1994), and preconditioned the exceptional production of deep Cretan waters in the following years (Klein et al., 1999; Malanotte-Rizzoli et al., 2003; Theocharis et al., 2002). However, the paradigm that the main source of LIW is the Levantine Sea, still verified in the “pre-Eastern Mediterranean Transient” observations (Malanotte-Rizzoli et al., 1997, 1999), is not followed in winter 2019, as the Cretan Sea became the prevalent source.

The thermohaline properties of intermediate waters identified during the winter of 2019 were scattered, covering the same range as that of previously reported wintertime values in the western Levantine Sea (Hainbucher et al., 2014; Klein et al., 1999; Roether et al., 1998; Sur et al., 1992; Wüst, 1961; Özsoy et al., 1989). The spatial and intra-seasonal variabilities of their properties were of the same order as interannual variability reported from previous studies, most likely because of the multiplicity of sources identified over the region during a single 3-month period.

5. Conclusion

The present study highlights the competition between two source regions, the Cretan Sea and the RCG, to supply the Mediterranean overturning circulation in LIW. During the winter 2019, effective subduction of LIW type waters was observed along the edges of RCG, with a nearby spreading and accumulation in the Cretan Passage. Meanwhile, a LIW type water outflow from the Cretan Sea was observed at the western Cretan strait. The two sources were amassed in the eastern Ionian Sea, and buffered there in order to regulate the LIW stocks constituted during wintertime with the all-year LIW supply to the overturning circulation. The Cretan source was estimated as the most abundant, supported by increasingly saltier water masses coming from the Levantine Sea. However, this winter 2019 situation was not exceptional, there are many similarities with the one described three decades ago (Malanotte-Rizzoli et al., 1999), but its enhanced documentation has revealed the Cretan source as the prevailing supplier of LIW. The relative contribution of the Cretan Sea in the paradigm that the main source of LIW is the Levantine Sea, might be reconsidered in the light of the present observation, and might have changed after the Eastern Mediterranean Transient.

This study confirms the efficiency of *in-situ* multiplatform approaches for accurately characterizing the dynamics of dense water formation zones. As previously carried out over the northwestern Mediterranean Sea, they have revealed the underlying sub-mesoscale processes of newly formed water spreading (Testor et al., 2018), and documented trends to salinification of the Mediterranean water source regions (Margirier et al., 2020). Contextualized by regional-scale field surveys based on cruises and a glider, the timeseries collected by profiling floats gave access to intra-seasonal changes in the hydrographical state of the RCG, from the preconditioning phase until the stratification phase, thus allowing a non-equivocal determination of the LIW, their properties, their origins and their fate.

Data Availability Statement

Data collected by the array of profiling floats were made freely available by the international Argo program and the national programs that contribute to it (Argo, 2000; <https://doi.org/10.17882/42182>). Data collected by the oceanographic cruises, profiling floats and the glider are available at the operational oceanographic data center Coriolis (<https://www.coriolis.eu.org/Data-Products/Data-Delivery/Mediterranean-Data-selection>).

Acknowledgments

This paper represents a contribution to the following research projects: NAOS (funded by the Agence Nationale de la Recherche in the framework of the French program “Equipement d’Avenir”, Grant No. ANR J11R107-F), “Chantier Méditerranée” MISTRALS-MERMEX (CNRS/INSU), DEKOSIM (BAP-08-11-DPT2012K120880) funded by the Turkish Ministry of Development, Argo-Italy funded by the Italian Ministry of Research, PROTEVS funded by the DGA, CLIMPACT and MARRE (TIEDK-02966) funded by the Public Investment Program of Greece. Thanks also go to the captains and crew of *R/V Tethys II* (CNRS/INSU), *Pourquoi Pas?* (IFREMER) and *L’Atalante* (IFREMER), for their participation to the deployment of autonomous platforms during the PERLE cruises.

References

- Argo. (2000). Argo float data and metadata from Global Data Assembly Centre (Argo GDAC). *SEANOE*. <https://doi.org/10.17882/42182>
- Astraldi, M., Balopoulos, S., Candela, J., Font, J., Gačić, M., Gasparini, G. P., et al. (1999). The role of straits and channels in understanding the characteristics of Mediterranean circulation. *Progress in Oceanography*, 44, 65–108. [https://doi.org/10.1016/S0079-6611\(99\)00021-X](https://doi.org/10.1016/S0079-6611(99)00021-X)
- Bensi, M., Velaoras, D., Meccia, V., & Cardin, V. (2016). Effects of the Eastern Mediterranean Sea circulation on the thermohaline properties as recorded by fixed deep-ocean observatories. *Deep-Sea Research I*, 112–113. <https://doi.org/10.1016/j.dsr.2016.02.015>
- Béthoux, J. P. (1980). Mean water fluxes across sections in the Mediterranean Sea, evaluated on the basis of water and salt budgets and of observed salinities. *Oceanologica Acta*, 3(1), 79–88.
- Béthoux, J. P., Gentili, B., Morin, P., Nicolas, E., Pierre, C., & Ruiz-Pino, D. (1999). The Mediterranean Sea: A miniature ocean for climatic and environmental studies and a key for the climatic functioning of the North Atlantic. *Progress in Oceanography*, 44, 131–146. [https://doi.org/10.1016/S0079-6611\(99\)00023-3](https://doi.org/10.1016/S0079-6611(99)00023-3)
- Béthoux, J. P., Morin, P., Chaumery, C., Connan, O., Gentili, B., & Ruiz-Pino, D. (1998). Nutrients in the Mediterranean Sea, mass balance and statistical analysis of concentrations with respect to environmental change. *Marine Chemistry*, 63, 155–169. [https://doi.org/10.1016/S0304-4203\(98\)00059-0](https://doi.org/10.1016/S0304-4203(98)00059-0)
- Bordone, A., Pennecchi, F., Raiteri, G., Repetti, L., & Reseghetti, F. (2020). XBT, ARGO float and ship-based CTD profiles intercompared under strict space-time conditions in the Mediterranean Sea: Assessment of metrological comparability. *Journal of Marine Science and Engineering*, 8, 313. <https://doi.org/10.3390/jmse8050313>
- Bosse, A., Testor, P., Damien, P., Estournel, C., Marsaleix, P., Mortier, L., et al. (2021). Wind-forced submesoscale symmetric instability around deep Convection in the northwestern Mediterranean Sea. *Fluids*. <https://doi.org/10.3390/fluids6030123>
- Bosse, A., Testor, P., Houpert, L., Damien, P., Prieur, L., Hayes, D., et al. (2016). Scales and dynamics of submesoscale coherent vortices formed by deep convection in the northwestern Mediterranean Sea. *Journal of Geophysical Research*. <https://doi.org/10.1002/2016JC012144>
- D’Ortenzio, F., Taillandier, V., Claustre, H., Prieur, L. M., Leymarie, E., Mignot, A., et al. (2020). Biogeochemical Argo: The test case of the NAOS Mediterranean array. *Frontiers in Marine Science*, 7, 120.
- D’Ortenzio, F., Iudicone, D., de Boyer Montegut, C., Testor, P., Antoine, D., Marullo, S., et al. (2005). Seasonal variability of the mixed layer depth in the Mediterranean Sea as derived from in situ profiles. *Geophysical Research Letters*. <https://doi.org/10.1029/2005GL022463>
- Durrieu de Madron, X., Guieu, C., Sempere, R., Conan, P., Cossa, D., D’Ortenzio, F., et al. (2011). Marine ecosystems’ responses to climatic and anthropogenic forcings in the Mediterranean. *Progress in Oceanography*, 91, 97–166. <https://doi.org/10.1016/j.pocean.2011.02.003>
- Fach, B. A., Orek, H., Yilmaz, E., Tezcan, D., Salihoglu, I., Salihoglu, B., & Latif, M. A. (2021). Water mass variability and levantine intermediate formation in the Eastern Mediterranean between 2015–2017. *Journal of Geophysical Research*. <https://doi.org/10.1029/2020JC016472>
- Feliks, Y. (1991). Downwelling along the northeastern coasts of the Eastern Mediterranean. *Journal of Physical Oceanography*, 21, 511–526.

- Gačić, M., Borzelli, G. L., Civitarese, G., Cardin, V., & Yari, S. (2010). Can internal processes sustain reversals of the ocean upper circulation? The Ionian Sea example. *Geophysical Research Letters*. <https://doi.org/10.1029/2010GL043216>
- Gačić, M., Schroeder, K., Civitarese, G., Cosoli, S., Vetrano, A., & Eusebi Borzelli, G. L. (2013). Salinity in the Sicily Channel corroborates the role of the Adriatic–Ionian Bimodal Oscillating System (BIOS) in shaping the decadal variability of the Mediterranean overturning circulation. *Ocean Science*, 9, 83–90. <https://doi.org/10.5194/os-9-83-2013>
- Gasparini, G. P., Ortona, A., Budillon, G., & Astraldi, M. (2005). The effect of the eastern Mediterranean transient on the hydrographic characteristics in the strait of Sicily and in the Tyrrhenian sea. *Deep Sea Research Part I Oceanographic Research Papers*, 52(6), 915–935. <https://doi.org/10.1016/j.dsr.2005.01.001>
- Georgopoulos, D., Theocharis, A., & Zodiatis, G. (1989). Intermediate Water formation in the Cretan Sea (south Aegean Sea). *Oceanologica Acta*, 12(4), 353–359.
- Gertman, I. F., Ovchinnikov, I. M., & Popov, Y. (1994). Deep convection in the eastern basin of the Mediterranean Sea. *Oceanology*, 34(1), 19–25.
- Hainbucher, D., Rubino, A., Cardin, V., Tahnuu, T., Schroeder, K., & Bensi, M. (2014). Hydrographic situation during cruise M84/3 and P414 (spring 2011) in the Mediterranean Sea. *Ocean Science*, 10, 669–682. <https://doi.org/10.5194/os-10-669-2014>
- Hecht, A., & Gertman, I. (2001). Physical features of the eastern Mediterranean resulting from the integration of POEM data with Russian Mediterranean cruises. *Deep-Sea Research I*, 48, 1847–1876.
- Hecht, A., Pinardi, N., & Robinson, A. (1988). Currents, water masses, eddies and jets in the Mediterranean Levantine Basin. *Journal of Physical Oceanography*, 18, 1320–1353.
- Hopkins, T. S. (1978). Physical processes in the Mediterranean basin. In B. Kjerfve (Ed.) *Estuarine transport processes* (pp. 269–310). University of South Carolina.
- Ioannou, A., Stegner, A., Le Vu, B., Taupier-Letage, I., & Speich, S. (2017). Dynamical evolution of intense Ierapetra eddies on a 22 year long period. *Journal of Geophysical Research: Oceans*. <https://doi.org/10.1002/2017JC013158>
- Kassis, D., & Korres, G. (2020). Hydrography of the Eastern Mediterranean basin derived from argo floats profile data. *Deep-Sea research II*. <https://doi.org/10.1016/j.dsr2.2019.104712>
- Klein, B., Roether, W., Manca, B., Bregant, D., Beitzel, V., Kovacevic, V., & Luchetta, A. (1999). The large deep water transient in the Eastern Mediterranean. *Deep-Sea Research I*, 46, 371–414.
- Kontoyiannis, H., Theocharis, A., Balopoulos, E., Kioroglou, S., Papadopoulos, V., Collins, M., et al. (1999). Water fluxes through the cretan arc straits, eastern Mediterranean Sea: March 1994 to June 1995. *Progress in Oceanography*, 44, 511–529.
- Kovacevic, V., Manca, B., Ursella, L., Schroeder, K., Cozzi, S., Burca, M., et al. (2012). Water mass properties and dynamic conditions of the Eastern Mediterranean in June 2007. *Progress in Oceanography*, 104, 59–79. <https://doi.org/10.1016/j.pocean.2012.05.006>
- Kress, N., Manca, B., Klein, B., & Deponte, D. (2003). Continuing influence of the changed thermohaline circulation in the eastern Mediterranean on the distribution of dissolved oxygen and nutrients: Physical and chemical characterization of the water masses. *Journal of Geophysical Research*, 108(C9), 8109. <https://doi.org/10.1029/2002JC001397>
- Krokos, G., Velaoras, D., Korres, G., Perivoliotis, L., & Theocharis, A. (2014). On the continuous functioning of an internal mechanism that drives the Eastern Mediterranean thermohaline circulation: The recent activation of the Aegean Sea as a dense water source area. *Journal of Marine Systems*, 129, 484–489. <https://doi.org/10.1016/j.jmarsys.2013.10.002>
- Kubin, E., Poulain, P. M., Mauri, E., Menna, M., & Notarstefano, G. (2019). Levantine intermediate and Levantine deep water formation: An argo float study from 2001 to 2017. *Water*. <https://doi.org/10.3390/w11091781>
- Lascaratos, A., Roether, W., Nittis, K., & Klein, B. (1999). Recent changes in deep Water formation and spreading in the eastern Mediterranean Sea: A review. *Progress in Oceanography*, 44, 5–36. [https://doi.org/10.1016/S0079-6611\(99\)00019-1](https://doi.org/10.1016/S0079-6611(99)00019-1)
- Malanotte-Rizzoli, P., Manca, B. B., d'Alcalà, M. R., Theocharis, A., Bergamasco, A., Bregant, D., et al. (1997). A synthesis of the Ionian Sea hydrography, circulation and water mass pathways during POEM-Phase I. *Progress in Oceanography*, 39, 153–204.
- Malanotte-Rizzoli, P., Manca, B. B., Marullo, S., Ribera d'Alcala, M., Roether, W., Theocharis, A., et al. (2003). The Levantine Intermediate Water Experiment (LIWEX) Group: Levantine basin – a laboratory for multiple water mass formation processes. *Journal of Geophysical Research*, 108(C9). <https://doi.org/10.1029/2002JC001643>
- Malanotte-Rizzoli, P., Manca, B. B., Ribera d'Alcalà, M., Theocharis, A., Brenner, S., Budillon, G., & Özsoy, E. (1999). The eastern Mediterranean in the 80's and in the 90's: The big transition in the intermediate and deep circulations. *Dynamics of Atmosphere and Oceans*, 29, 365–395.
- Malanotte-Rizzoli, P., Robinson, A. R., Roether, W., Manca, B., Bergamasco, A., Brenner, S., et al. (1996). Experiment in the eastern Mediterranean probes the origin of deep water masses. *Eos, Transactions American Geophysical Union*, 77(32), 305–307.
- Manca, B. B., Budillon, G., Scarazzato, P., & Ursella, L. (2003). Evolution of dynamics in the eastern Mediterranean affecting water mass structures and properties in the Ionian and Adriatic Seas. *Journal of Geophysical Research*. <https://doi.org/10.1029/2002JC001664>
- Margirier, F., Testor, P., Heslop, E., Mallil, K., Bosse, A., Houpert, L., et al. (2020). Abrupt warming and salinification of intermediate waters interplays with decline of deep convection in the Northwestern Mediterranean Sea. *Nature Scientific Reports*, 10, 20923. <https://doi.org/10.1038/s41598-020-77859-5>
- Marullo, S., Napolitano, E., Santoleri, R., Manca, B., & Evans, R. (2003). Variability of Rhodes and Ierapetra gyres during Levantine intermediate water experiment: Observations and model results. *Journal of Geophysical Research*. <https://doi.org/10.1029/2002JC001393>
- Mauri, E., Sitz, L., Gerin, R., Poulain, P.-M., Hayes, D., & Gildor, H. (2019). On the variability of the circulation and water mass properties in the Eastern Levantine Sea between September 2016–August 2017. *Water*, 11(9), 1741. <https://doi.org/10.3390/w11091741>
- Menna, M., Gerin, R., Notarstefano, G., Mauri, E., Bussani, A., Pacciaroni, M., & Poulain, P.-M. (2021). On the circulation and thermohaline properties of the Eastern Mediterranean Sea. *Frontiers in Marine Science*, 8, 671469. <https://doi.org/10.3389/fmars.2021.671469>
- Moutin, T., & Prieur, L. (2012). Influence of anticyclonic eddies on the biogeochemistry from the oligotrophic to the ultraoligotrophic Mediterranean (BOUM Cruise). *Biogeosciences*. <https://doi.org/10.5194/bg-9-3827-2012>
- Nielsen, J. N. (1912). Hydrography of the Mediterranean and adjacent waters. In *Report of the Danish Oceanographic Expedition 1908-1910 to the Mediterranean and Adjacent waters*. (Vol. 1, pp. 72–191).
- Özsoy, E., Hecht, A., & Unluata, U. (1989). Circulation and hydrography of the Levantine Basin. Results of POEM coordinated experiments 1985–1986. *Progress in Oceanography*, 22, 125–170.
- Özsoy, E., Hecht, A., Unluata, U., Brenner, S., Sur, H. I., Bishop, J., et al. (1993). A synthesis of Levantine basin circulation and hydrography 1985 – 1990. *Deep-Sea Research II*, 40, 1075–1120.
- Pinardi, N., Cessi, P., Borile, F., & Wolfe, C. L. P. (2019). The Mediterranean Sea overturning circulation. *Journal of Physical Oceanography*. <https://doi.org/10.1175/JPO-D-18-0254.1>

- Pinardi, N., Zavatarelli, M., Adani, M., Coppini, G., Fratianni, C., Oddo, P., et al. (2015). Mediterranean Sea large-scale low-frequency ocean variability and water mass formation rates from 1987 to 2007: A retrospective analysis. *Progress in Oceanography*. <https://doi.org/10.1016/j.pocean.2013.11.003>
- Pond, S., & Pickard, G. L. (1983). *Introductory dynamical oceanography*. Elsevier. <https://doi.org/10.1016/C2009-0-24288-7>
- Popov, Y. I. (2004). Genesis and structure of the anticyclonic Ierapetra zone in the Levantine basin. *Physical Oceanography*, 14(4), 234–242.
- Poulain, P. M. (2001). Adriatic Sea surface circulation as derived from drifter data between 1990 and 1999. *Journal of Marine Systems*. [https://doi.org/10.1016/S0924-7963\(01\)00007-0](https://doi.org/10.1016/S0924-7963(01)00007-0)
- Poulain, P. M., Barbanti, R., Font, J., Cruzado, A., Millot, C., Gertman, I., et al. (2007). MedArgo: A drifting profiler program in the Mediterranean Sea. *Ocean Science*, 3, 379–395.
- Prieur, L., D'Ortenzio, F., Taillandier, V., & Testor, P. (2020). Physical oceanography of the Ligurian sea. In C. Migon, A. Sciandra, & P. Nival (Eds.), *The Mediterranean sea in the era of global change (volume 1), evidence from 30 years of multidisciplinary study of the Ligurian sea*. ISTE Science Publications Ltd. (pp. 49–78). <https://doi.org/10.1002/9781119706960.ch3>
- Pujo-Pay, M., Conan, P., Oriol, L., Cornet-Barthaux, V., Falco, C., Ghiglione, J.-F., et al. (2011). Integrated survey of elemental stoichiometry (C, N, P) from the Western to eastern Mediterranean Sea. *Biogeosciences*, 8, 1–17. <https://doi.org/10.5194/bg-8-1-2011>
- Ribera d'Alcalà, M., Civitarese, G., Conversano, F., & Lavezza, R. (2003). Nutrient ratios and fluxes hint at overlooked processes in the Mediterranean Sea. *Journal of Geophysical Research*, 108, 8106. <https://doi.org/10.1029/2002JC001650>
- Robinson, A. R., Golnaraghi, M., Leslie, W. G., Artegiani, A., Hecht, A., Lazzoni, E., et al. (1991). The eastern Mediterranean general circulation: Features, structure and variability. *Dynamics of Atmosphere and Oceans*, 15, 215–240. [https://doi.org/10.1016/0377-0265\(91\)90021-7](https://doi.org/10.1016/0377-0265(91)90021-7)
- Roemmich, D., Alford, M. H., Claustre, H., Johnson, K., King, B., Moum, J., et al. (2019). On the future of argo: A global, full-depth, multi-disciplinary array. *Frontiers in Marine Science*, 6, 439. <https://doi.org/10.3389/fmars.2019.00439>
- Roether, W., Klein, B., Beitzel, V., & Manca, B. (1998). Property distributions and transient-tracer ages in Levantine intermediate water in the eastern Mediterranean. *Journal of Marine Systems*, 18, 71–87.
- Schroeder, K., Chiggiato, J., Josey, S. A., Borghini, M., Aracri, S., & Sparnocchia, S. (2017). Rapid response to climate change in a marginal sea. *Nature Scientific Reports*, 7, 4065. <https://doi.org/10.1038/s41598-017-04455-5>
- Schroeder, K., Cozzi, S., Belgacem, M., Borghini, M., Cantoni, C., Durante, S., et al. (2020). Along-path evolution of biogeochemical and carbonate system Properties in the intermediate water of the Western Mediterranean. *Frontiers in Marine Science*, 7, 375. <https://doi.org/10.3389/fmars.2020.00375>
- Simoncelli, S., Fratianni, C., Pinardi, N., Grandi, A., Drudi, M., Oddo, P., & Dobricic, S. (2018). *Mediterranean Sea physical reanalysis (MEDREA 1987-2015)*. Copernicus Monitoring Environment Marine Service. https://doi.org/10.25423/medsea_reanalysis_phys_006_004
- Sur, H. L., Özsoy, E., & Unluata, U. (1992). Simultaneous deep and intermediate depth convection in the Northern Levantine Sea, winter 1992. *Oceanologica Acta*, 16(1), 33–43.
- Taillandier, V., Wagener, T., D'Ortenzio, F., Mayot, N., Legoff, H., Ras, J., et al. (2018). Hydrography and biogeochemistry dedicated to the Mediterranean BGC-Argo network during a cruise with RV Tethys 2 in May 2015. *Earth System Science Data*, 10(1), 627–641. <https://doi.org/10.5194/essd-10-627-2018>
- Testor, P., Bosse, A., Houpert, L., Margirier, F., Mortier, L., Legoff, H., et al. (2018). Multiscale observations of deep convection in the north-western Mediterranean Sea during winter 2012–2013 using multiple platforms. *Journal of Geophysical Research: Oceans*. <https://doi.org/10.1002/2016JC012671>
- Testor, P., de Young, B., Rudnick, D. L., Glenn, S., Hayes, D., Lee, C. M., et al. (2019). OceanGliders: A component of the integrated GOOS. *Frontiers in Marine Science*, 6, 422. <https://doi.org/10.3389/fmars.2019.00422>
- Theocharis, A., Balopoulos, E., Kioroglou, S., Kontoyiannis, H., & Iona, A. (1999). A synthesis of the circulation and hydrography of the south Aegean Sea and the straits of the Cretan Arc (March 1994 – January 1995). *Progress in Oceanography*, 44(4), 469–509. [https://doi.org/10.1016/S0079-6611\(99\)00041-5](https://doi.org/10.1016/S0079-6611(99)00041-5)
- Theocharis, A., Georgopoulos, D., Lascaratos, A., & Nittis, K. (1993). Water masses and circulation in the central region of the eastern Mediterranean: Eastern Ionian, south Aegean and northwest Levantine, 1986–1987. *Deep-Sea Research Part II*, 40(6), 1121–1142. [https://doi.org/10.1016/0967-0645\(93\)90064-T](https://doi.org/10.1016/0967-0645(93)90064-T)
- Theocharis, A., Klein, B., Nittis, K., & Roether, W. (2002). Evolution and status of the eastern Mediterranean transient (1997–1999). *Journal of Marine Systems*, 33, 91–116. [https://doi.org/10.1016/S0924-7963\(02\)00054-4](https://doi.org/10.1016/S0924-7963(02)00054-4)
- Theocharis, A., Krokos, G., Velaoras, D., & Korres, G. (2014). An internal mechanism driving the alternation of the Eastern Mediterranean dense/deep water sources. In G. L. E. Borzelli, M. Gagic, P. Lionello, P. Malanotte-Rizzoli (Eds.), *The Mediterranean Sea: Temporal variability and spatial patterns*, AGU Geophysical Monograph Series (Vol. 202, pp. 113–137). John Wiley. <https://doi.org/10.1002/9781118847572.ch8>
- Troupin, C., Barth, A., Sirjacobs, D., Ouberdous, M., Brankart, J. M., Brasseur, P., et al. (2012). Generation of analysis and consistence error fields using data interpolating variational analysis (DIVA). *Ocean Modelling*, 52–53. <https://doi.org/10.1016/j.ocemod.2012.05.002>
- Tsimplis, M. N., Zervakis, V., Josey, S., Peneva, E., Struglia, M., Stanev, E., et al. (2006). Changes in the oceanography of the Mediterranean Sea and their link to climate variability. *Developments in Earth and Environmental Sciences*, 4, 227–282. [https://doi.org/10.1016/S1571-9197\(06\)80007-8](https://doi.org/10.1016/S1571-9197(06)80007-8)
- Velaoras, D., Krokos, G., Nittis, K., & Theocharis, A. (2014). Dense intermediate water out-flow from the Cretan Sea: A salinity driven, recurrent phenomenon, connected to thermohaline circulation changes. *Journal of Geophysical Research: Oceans*. <https://doi.org/10.1002/2014JC009937>
- Velaoras, D., Papadopoulos, V., Kontoyiannis, H., Cardin, V., & Civitarese, G. (2019). Water masses and hydrography during April and June 2016 in the Cretan Sea and Cretan passage (eastern Mediterranean Sea). *Deep-Sea Research II*. <https://doi.org/10.1016/j.dsr2.2018.09.005>
- Velaoras, D., Papadopoulos, V. P., Kontoyiannis, H., Papageorgiou, D. K., & Pavlidou, A. (2017). The response of the Aegean Sea (Eastern Mediterranean) to the extreme 2016–2017 winter. *Geophysical Research Letters*, 44(18), 9416–9423. <https://doi.org/10.1002/2017GL074761>
- Waldman, R., Brüggemann, N., Bosse, A., Spall, M., Somot, S., & Sevault, F. (2018). Overturning the Mediterranean thermohaline circulation. *Geophysical Research Letters*, 45(16), 8407–8415. <https://doi.org/10.1029/2018GL078502>
- Williams, R. G., & Follows, M. J. (2003). Physical transport of nutrients and the maintenance of biological production. In M. J. R. Fasham (Ed.), *Ocean biogeochemistry, Global Change – the IGBP Series*, Springer.
- Wong, A., Keeley, R., Carval, T., & The Argo data Management Team. (2019). Argo quality control manual for CTD and trajectory Data. <https://doi.org/10.13155/33951>
- Wüst, G. (1961). On the vertical circulation of the Mediterranean Sea. *Journal of Geophysical Research*, 66(10), 3261–3271.